Clim Dyn (2012) 39:1021–1042
DOI 10.1007/s00382-012-1432-y

Decadal-timescale changes of the Atlantic overturning circulation and climate in a coupled climate model with a hybrid-coordinate ocean component

A. Persechino · R. Marsh · B. Sinha · A. P. Megann · A. T. Blaker · A. L. New

Received: 3 May 2011 / Accepted: 19 June 2012 / Published online: 11 July 2012

Abstract A wide range of statistical tools is used to investigate the decadal variability of the Atlantic Meridional Overturning Circulation (AMOC) and associated key variables in a climate model (CHIME, Coupled Hadley-Isopycnic Model Experiment), which features a novel ocean component. CHIME is as similar as possible to the 3rd Hadley Centre Coupled Model (HadCM3) with the important exception that its ocean component is based on a hybrid vertical coordinate. Power spectral analysis reveals enhanced AMOC variability for periods in the range 15–30 years. Strong AMOC conditions are associated with: (1) a Sea Surface Temperature (SST) anomaly pattern reminiscent of the Atlantic Multi-decadal Oscillation (AMO) response, but associated with variations in a northern tropical-subtropical gradient; (2) a Surface Air Temperature anomaly pattern closely linked to SST; (3) a positive North Atlantic Oscillation (NAO)-like pattern; (4) a northward shift of the Intertropical Convergence Zone. The primary mode of AMOC variability is associated with decadal changes in the Labrador Sea and the Greenland Iceland Norwegian (GIN) Seas, in both cases linked to the tropical activity about 15 years earlier. These decadal changes are controlled by the low-frequency NAO that may be associated with a rapid atmospheric teleconnection from the tropics to the extratropics. Poleward advection of salinity anomalies in the mixed layer also leads to AMOC changes that are linked to processes in the Labrador Sea. A secondary mode of AMOC variability is associated with interannual changes in the Labrador and GIN Seas, through the impact of the NAO on local surface density.

Keywords Atlantic Meridional Overturning Circulation · North Atlantic Oscillation · Coupled climate model · Isopycnal · Decadal variability

A. Persechino (✉) · R. Marsh
Ocean and Earth Science, University of Southampton, European Way, Southampton, Hampshire SO14 3ZH, UK
e-mail: a.persechino@noc.soton.ac.uk

B. Sinha · A. P. Megann · A. T. Blaker · A. L. New
National Oceanography Centre, European Way, Southampton, Hampshire SO14 3ZH, UK

1 Introduction

Substantial climate variability of the North Atlantic-European region occurs on timescales of decades, and is thought to be associated with fluctuations in the large-scale meridional overturning of the ocean (Gordon et al. 1992). This Atlantic meridional overturning circulation (AMOC) is known to have a prominent influence on the North Atlantic climate (e.g. Winton 2003; Herweijer et al. 2005) through its contribution to the large poleward heat transport (e.g. Latif et al. 2004). With the current focus on rapid changes in the AMOC attributed to global warming, it is important to understand the natural decadal variability associated with the AMOC and climate, as this is the timescale on which we are now seeking the fingerprints of anthropogenic climate change (Santer et al. 1996).

Because of the limited availability of sufficiently long instrumental records, numerical models must be used to understand the principal mechanisms of decadal climate variability. There are indications that the current generation of climate models can indeed simulate aspects of decadal to multidecadal climate variability, as seen in the instrumental record (Knight et al. 2005) and proxy data (Delworth and Mann 2000). Although these oscillations are mostly irregular and their periods change considerably between models (varying between 25 and 80-year periods),

this internal climate variability on decadal to multidecadal timescales is generally attributed to fluctuations in the AMOC.

Some studies show that decadal variability is due to an active coupling between ocean and atmosphere, while others associate it with a damped ocean-only mode, excited by atmospheric noise. For example, some modelling studies found that mechanisms responsible for decadal variability of the AMOC are associated with a pure damped oceanic mode excited by atmospheric forcing which is related to changes in the strength of the subpolar gyre (e.g. Delworth et al. 1993; Jungclaus et al. 2005; Dong and Sutton 2005) or with changes in convection in the Nordic Seas (Hawkins and Sutton 2007). By contrast, others have found clear evidence of active coupling between the ocean and the atmosphere, either related to the Norh Atlantic Oscillation (NAO) (e.g. Timmerman et al. 1998; Danabasoglu 2008) or to the Intertropical Convergence Zone (ITCZ) (e.g. Vellinga and Wu 2004). There is also some uncertainty concerning the relative role of freshwater export from the high-latitudes (e.g. Hawkins and Sutton 2007) and tropical processes (Vellinga and Wu 2004; Mignot and Frankignoul 2005) in explaining multi-decadal fluctuations of the AMOC. For example, Vellinga and Wu (2004) suggested that the reversal of these AMOC oscillations is triggered by an anomalous advection of salinity from the tropics, while Hawkins and Sutton (2007) argued that the main salinity feedback comes from the Arctic. Although a distinction between variability on longer (50–70 year) and shorter (20–30 year) multi-decadal timescales has recently led to some clarification of AMOC dynamics and climate system processes (Frankcombe et al. 2010), mechanisms responsible for decadal variability of the AMOC are still under debate. From a perspective of developing operational decadal prediction schemes, improving our understanding of such variability is therefore prerequisite.

In this paper, we focus on the shorter timescale (i.e. 15–30 years, referring to the associated variability as "decadal"), and describe the natural variability of the AMOC and associated key variables in a new climate model, CHIME. A brief description of the model and data is given in Sect. 2. In Sect. 3, we describe the structure and variability of the AMOC in CHIME. Co-variability of ocean properties and surface climate are discussed in Sect. 4. Underlying physical mechanisms are considered in Sect. 5. A summary and discussion follow in Sect. 6, with concluding remarks in Sect. 7.

2 Model and experiment descriptions

2.1 Model description

The model we use is the Coupled Hadley-Isopycnic Model Experiment (CHIME), which is described by Megann et al. (2010). CHIME is a new coupled climate model that features an innovative hybrid coordinate in the ocean, but is otherwise identical to a widely used IPCC-class model, HadCM3 (3rd Hadley Centre Coupled Model, Gordon et al. 2000). It comprises the atmosphere and ice components of HadCM3, coupled to version *2.1.34* of the hybrid coordinate ocean model, HYCOM (Bleck 2002). There is no flux correction. The atmosphere has a horizontal resolution of 3.75° east–west and 2.5° north–south, and uses a hybrid vertical coordinate with 19 vertical levels. The ocean component of CHIME uses a "spherical-bipolar" grid (similar to that described by Sun and Bleck 2001) composed of two regions: (1) from 78°S to 55°N it has a constant angular resolution of 1.25° × 1.25° and (2) north of 55°N the spherical grid is matched smoothly to a bipolar grid with poles situated at (55°N, 110°W) and (55°N, 70°E), with resolutions at ocean points between 40 and 140 km. HYCOM has 25 vertical layers combining isopycnic layers (each with constant potential density σ_2 referred to 2,000 dbar) in the ocean interior, with constant depth layers near the surface.

2.2 Model experiment

The results presented in this paper are based on an analysis of a 200-year run with preindustrial atmospheric CO_2 and aerosol levels, enabling us to isolate the internal variability of the model under constant external forcing. It is initialized from the full-depth Levitus (1998) autumn climatology with an atmospheric initial state identical to that in the HadCM3 model experiment (described by Gordon et al. 2000), and output is stored at monthly-mean time resolution. CHIME is run in fully coupled mode from rest. A spin-up time is clearly identified up to year 80 as seen in the time series of the AMOC index (Fig. 1a, black line, further described in Sect. 3.1); we will therefore restrict our analyses starting from this year despite a trend of about -1.5 Sv century^{-1} thereafter. CHIME simulates realistic ocean heat transports and overturning circulation, and has a generally realistic climate (Megann et al. 2010).

2.3 Diagnostics and study area

Data analyzed here comprise the annual-mean meridional mass transport streamfunction of the Atlantic averaged over 121 years of integration (from year 80 to 200), and an AMOC index defined as its maximum at 30°N. We also analyze ocean fields such as salinity, temperature, surface potential density with respect to the 2,000 dbar surface (a measure of static stability), mixed layer depth (MLD), surface heat and freshwater fluxes, and atmospheric fields such as surface air temperature (SAT), sea level pressure (SLP), and net precipitation. Because of the "spherical-

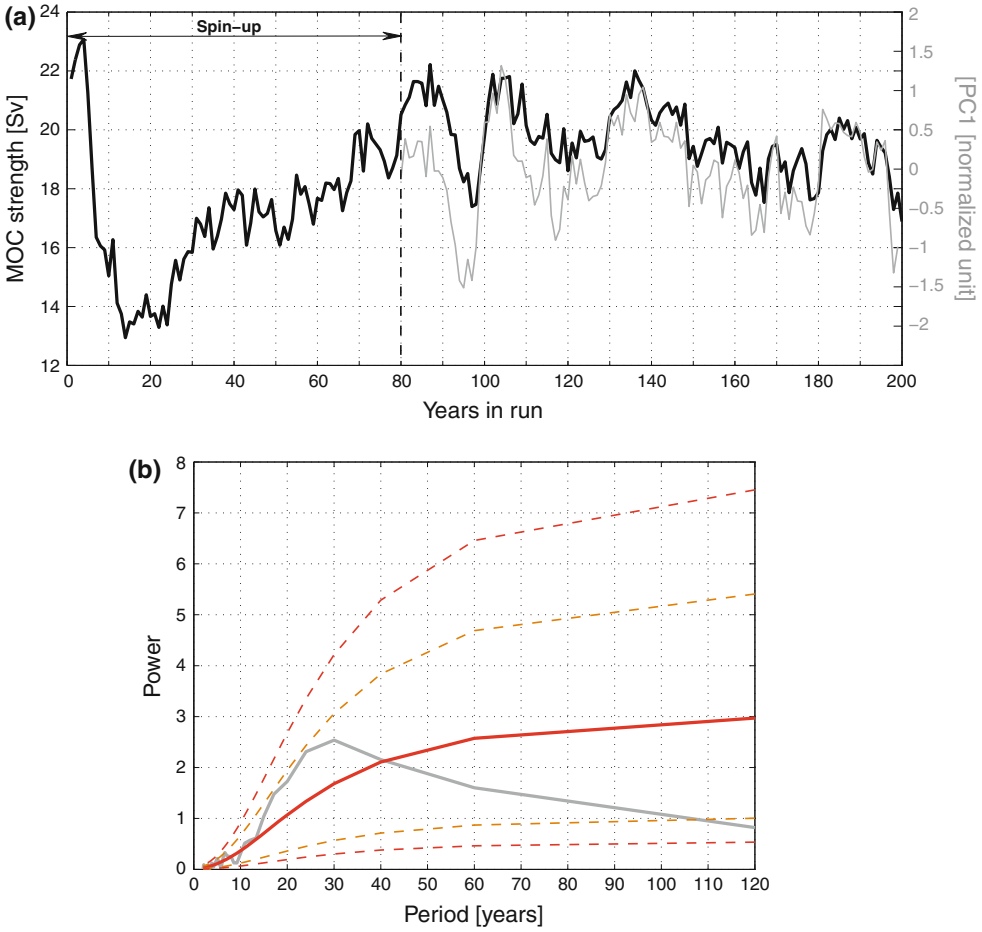

Fig. 1 **a** Time series of the AMOC index for the whole 200-year simulation (*black line*) superimposed onto the PC1 time series of the AMOC streamfunction from year 80 (*grey line*), **b** Power Spectrum of the detrended PC1 (*grey line*) using the Welch method of spectra estimation. The smooth *red solid line* is the power of a red noise spectrum with the same AR(1) coefficient fitted from the detrended PC1 time series, and *red* (*orange*) *dashed lines*, which are the 95 % (80 %) confidence limits

bipolar" grid used in the ocean component of CHIME, ocean fields have been re-gridded onto a regular 1.25° × 1.25° grid north of 55°N.

Throughout the present study, we either use annual means, winter means (January–March) or September values for the different fields. Winter means are used to characterise activities in the high-latitude regions (as deep water is formed by convection in these regions mainly during the cold winter seasons) while September means characterise processes specific to the tropical regions (coincident with heaviest precipitation in the central Atlantic, at around the time of the northernmost position of the ITCZ). Note that the use of winter or September means does not give qualitatively different results to the use of annual means but rather strengthens statistical robustness in some cases. When focusing on low-frequency variability, we apply 5- or 10-year moving average filters to the data. Significance of correlations and regressions are tested using a Student's t test at either 90 or 95 % confidence level. Significance of anomalies are tested using a z test at the 90 % confidence level.

The domain of study for the present analysis is the Atlantic sector between 20°S–80°N and 90°W–30°E. We further consider regions where deep convection occurs in the model. The maximum MLD in March defines the deep convection sites as shown in Fig. 2. Three deep convection sites are evident: (1) the Greenland-Iceland-Norwegian Seas (hereinafter GIN Seas), (2) the Labrador Sea and (3) a

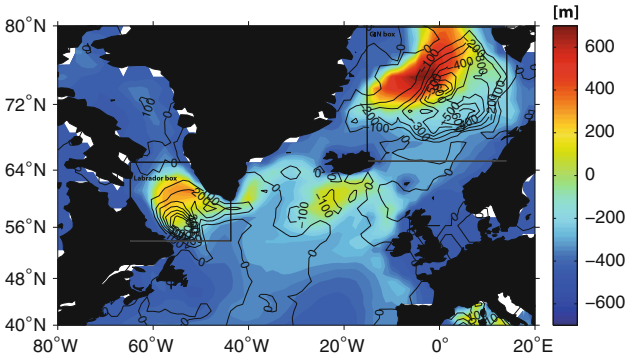

Fig. 2 March Mixed Layer Depth [m] averaged from year 80 to 200 and superimposed onto its regression coefficients onto PC1 of the AMOC streamfunction represented as *contours* [m Sv^{-1}]. The Labrador (GIN) Sea(s) box is defined as 55°N–65°N/45°W–65°W (65°N–80°N/15°W–15°E)

small region south of Iceland (extending down to about 57°N). Deep convection in the latter is significantly less than in the Labrador and GIN Seas. Furthermore, the Labrador and GIN Seas are both regions where MLD and AMOC fluctuations are most sensitively related (>200 m Sv^{-1}). We therefore focus analysis on these two main regions, for which the Labrador and GIN Seas domains have been respectively defined as 55°N–65°N/45°W–65°W and 65°N–80°N/15°E–15°W (see boxes, Fig. 2). Respective convective indices have been calculated from the annual winter-mean MLD averaged over the corresponding domains.

3 Internal AMOC variability in CHIME

3.1 Spin-up, trend and variability of the AMOC

The AMOC index time series is shown for the entire run in Fig. 1a (black line). From year 80, decadal-to-multidecadal timescale variability is easily distinguished from the spinup transient. The amplitude of variability is about 2 Sv (ranging from 17.5 to 22 Sv). The average decadal mean (about 19.8 ± 1.4 Sv) compares well with observational estimates (18 ± 2–3 Sv) of Talley (2003), but is a little smaller than the mean of 22.8 ± 1.6 Sv in the corresponding period of HadCM3 (Megann et al. 2010). The principal component associated with the main mode of variability of the AMOC streamfunction (PC1, further discussed in Sect. 3.2) is superimposed on the AMOC index (Fig. 1a, grey line). The two time series are highly correlated, with correlation coefficient of 0.86 (Table 1). Although its corresponding power spectrum shows most energy (relative to a fitted first order autoregressive AR1 model, Chatfield 1975) at a period of about 30 years, this is well below the 80 % confidence limit about the fitted red noise spectrum (Fig. 1b). Although not significant, periods in the range 15–30 years almost reach this 80 % confidence limit, so it appears that the PC1 of the AMOC in CHIME reveals an enhanced power compared to a fitted red noise spectrum for periods in this range.

The mean AMOC streamfunction (Fig. 3) has similar features to the mean AMOC inferred from observations (Ganachaud and Wunsch 2000); the circulation associated with the North Atlantic Deep Water (NADW) has a maximum transport of about 18 Sv at a depth of 800–1,200 m occurring at about 30°N. NADW lies at a maximum depth of about 4,000 m, which is considerably deeper than the observed depth at which NADW enters the Deep Western Boundary Current (about 2,000–2,500 m, Reid 1989). This bias could be the result of either the weakened Antarctic Bottom Water (AABW) cell found in CHIME (Megann et al. 2010) or an unrealistic degree of preservation of the density outflows from the Nordic Seas as a consequence of the isopycnic coordinate system (Roberts et al. 1996) that will result in a too-dense NADW cell. The 18 Sv of warm northward flow is found in the upper ocean (mainly in the Gulf Stream and North Atlantic Current) with the strongest sinking occurring in a broad region between about 55°N and 65°N. There is also evidence for deep water formation in the Nordic Seas as far as 70°N. The inflow of AABW (the reverse cell below 4,000 m) reaches barely 2 Sv; Megann et al. (2010) suggest that this is due to excessive wintertime ice cover in the Antarctic and hence insufficient heat loss to form realistic volumes of bottom water.

3.2 EOF analysis of AMOC variability

To analyze the spatial patterns associated with variability of the AMOC in CHIME, we have calculated EOFs (e.g. von Storch and Zwiers 1999) based on 121 years of annual-mean AMOC streamfunction calculated from year 80 onwards (Fig. 4). Prior to the calculations, time series are normalized by the variance, and detrended.

EOF1 explains 33.6 % of the total variance (Fig. 4a), and has a basin-wide structure similar to that of the streamfunction itself (Fig. 3). It has a maximum value of about 1.6 Sv (for a fluctuation of one standard deviation of PC1) with the strongest sinking taking place primarily at about 55–60°N. As already mentioned in Sect. 3.1, PC1 (Fig. 4b, black line) shows an enhanced power for periods in the range 15–30 years and is significantly correlated

Table 1 Maximum correlation coefficients between 10-year moving averages of the PC1 of AMOC and several different variables

Variable	Max correlation coefficient	Lag (years)
AMOC index	**0.86**	Instantaneous
September northern tropical-subtropical SST gradient	**0.79**	Near-instantaneous
Convective index (Labrador)	**0.90**	PC1 lags by ~2
Convective index (GIN)	**−0.70**	PC1 lags by ~1
Winter surface potential density (Labrador)	**0.86**	PC1 lags by ~2
Winter surface potential density (GIN)	**−0.83**	PC1 lags by ~1
Tropical activity (TA)	**0.75**	PC1 lags by ~8–9

Bold correlations are statistically significant at the 90 % confidence limits

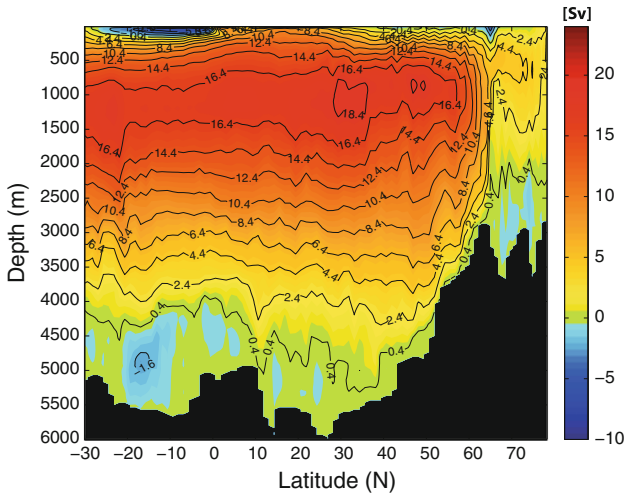

Fig. 3 Annual mean streamfunction of zonally integrated volume transport [Sv] from 30°S to 80°N, averaged from years 80 to 200 in CHIME. Positive values mean clockwise circulation

with the AMOC index; we shall therefore use PC1 of the AMOC as a reference time series in the following analyses. It would therefore seem that EOF1 thus describes AMOC changes associated with variability in the period range 15–30 years, most likely related to Labrador Sea Water (LSW) variability; the strongest sinking indeed occurs at about 55–60°N and PC1 shows a close link with convective activity (MLD) in the Labrador Sea (Fig. 4b, red line). However, convective activity in the GIN Seas also seems to be closely linked to PC1 of the AMOC as seen by their apparent anti-phase relationship (Fig. 4b, blue line). These close relationships between the AMOC and convective activities are further investigated in Sect. 5. It is clear, therefore, that EOF1, which shows the principal changes happening in the AMOC on decadal timescales, appears to capture not only the mechanism associated with LSW variability but also mechanisms associated with variability in the GIN Seas.

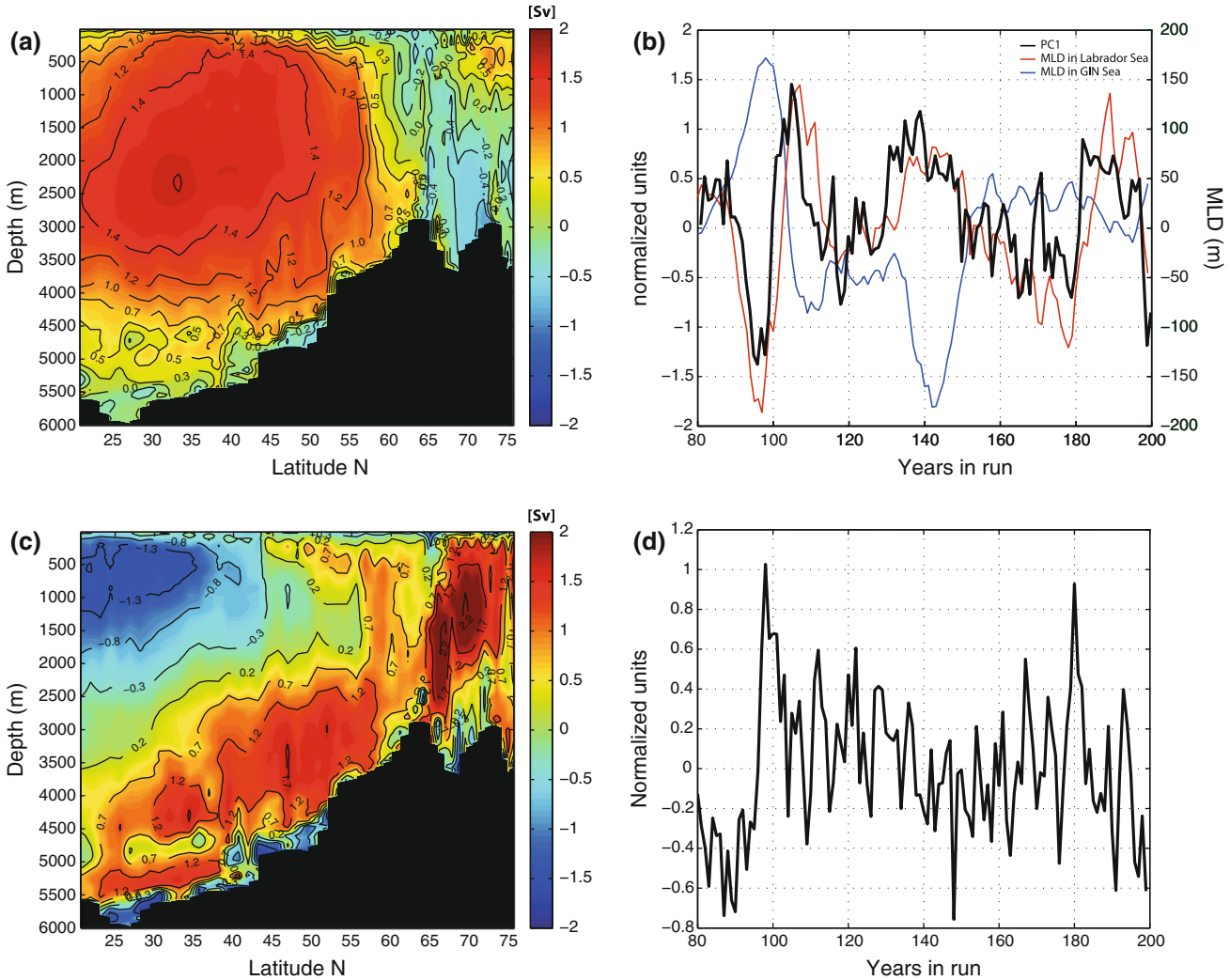

Fig. 4 Detrended AMOC streamfunction (from year 80 to 200) in the North Atlantic (20°N–75°N): **a** EOF1; **b** PC1 (*black line*) and 10-year moving average winter MLD in Labrador Sea (*red line*) and GIN Seas (*blue line*); **c** EOF2 and **d** PC2

One further interesting feature of EOF1 is the anti-phase relationship between latitude ranges corresponding to the Labrador Sea and to the Nordic Seas (Fig. 4a), which is confirmed by the clear anti-correlation between convective activities in these two regions (Fig. 4b). In observational studies, convection in the Labrador Sea has indeed generally been found to vary out of phase with convection in the Greenland Sea (Dickson et al. 1996; Hurrell and Dickson 2004). However, this is not the case for all climate models, for example HadCM3 (e.g. Dong and Sutton 2005; Bingham et al. 2007) has generally weak convection in the Labrador Sea (possibly related to the substantial surface freshening that occurs in the subpolar gyre of that model). Mechanisms behind this anti-phase pattern in CHIME will be further investigated in Sect. 5.

EOF2, which accounts for about 12 % of the total variance, shows a dipole pattern with mainly positive values from 40°N to 75°N below 2,500 m, and negative values in the upper ocean south of 40°N (Fig. 4c). The strongest variability in the sinking here takes place primarily at about 55–65°N and 65–70°N. The positive cell of EOF2 may arise through deeper sinking and return flow in the upper cell of the AMOC; this could be related to changes in surface winds and/or surface fluxes in the GIN Seas, leading to an increase in the density of the overflow waters. The strong amplitude of this second mode of AMOC variability close to the ocean bottom in the subpolar region and north of the sills suggests a role for both the denser LSW and Greenland Sea Water (GSW), and that these latter vary on interannual rather than decadal timescales (see Fig. 4d). We note that PC2 also shows evidence of multi-decadal variability but a longer simulation would be needed to confirm this.

From this EOF analysis, we develop the following picture of the AMOC streamfunction and its evolution in time: a primary mode of variability is associated with a decadal cycle related to convective activity in the Labrador and (inversely) the GIN Seas, while a secondary mode is rather associated with interannual variability of convective activity in these two regions. Note that, as shown by the standard deviation of the streamfunction in Fig. 5, the strongest AMOC fluctuations occur within the NADW cell at the latitude range of the Labrador Sea (50–60°N) and to a lesser extent in the GIN Seas at about 70–75°N.

3.3 Evolution of the AMOC on a decadal timescale

To further examine the decadal variability of the AMOC, lead-lag regressions of the AMOC streamfunction on PC1 of the AMOC have been calculated and are shown in Fig. 6. Because of the short control experiment length, most of the coefficients are not statistically significant (grey shading, Fig. 6). Nevertheless, this figure still gives useful indications about the dynamical evolution of the decadal AMOC

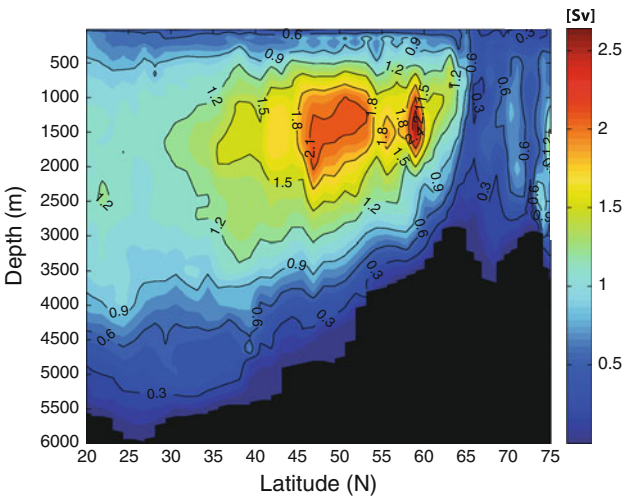

Fig. 5 Standard deviation of the annual mean streamfunction shown in Fig. 3 [Sv]

oscillation in CHIME. At lag −15 years, we found evidence for the NADW cell to be in its weak phase with an anti-clockwise anomalous circulation. Gradually, significant positive anomalies of meridional circulation develop in the tropics and extend northwards. At lag 0, the AMOC reaches a maximum with enhanced northward warm surface flow, stronger southward deep return flow, and enhanced downwelling at about 55–60°N. Thereafter, positive anomalies of meridional circulation gradually weaken and negative anomalies begin to appear in the tropics. Note that both EOF1 and EOF2 patterns of the AMOC are clearly identifiable here (e.g. at lag 0 and +6, respectively), underlining the contribution of these two modes to decadal variability of the AMOC. On a decadal timescale, streamfunction anomalies responsible for the reversal of phase of the AMOC oscillation in CHIME seem to originate in low latitudes. The possibility that they may even originate in the South Atlantic through compensation in the flow of NADW across the Equator (Schmitz and Richardson 1991) is not excluded. We note a link between the development of streamfunction anomalies in the low latitudes, and the associated northward transport of salinity anomalies (see Sect. 5.3.1).

4 Associated signals and impacts

The associated signals and impacts of AMOC variability in CHIME are considered in the ocean and the atmosphere respectively.

4.1 Ocean

A composite of winter sea surface temperature (SST) anomaly patterns (relative to the year 80–200 winter mean)

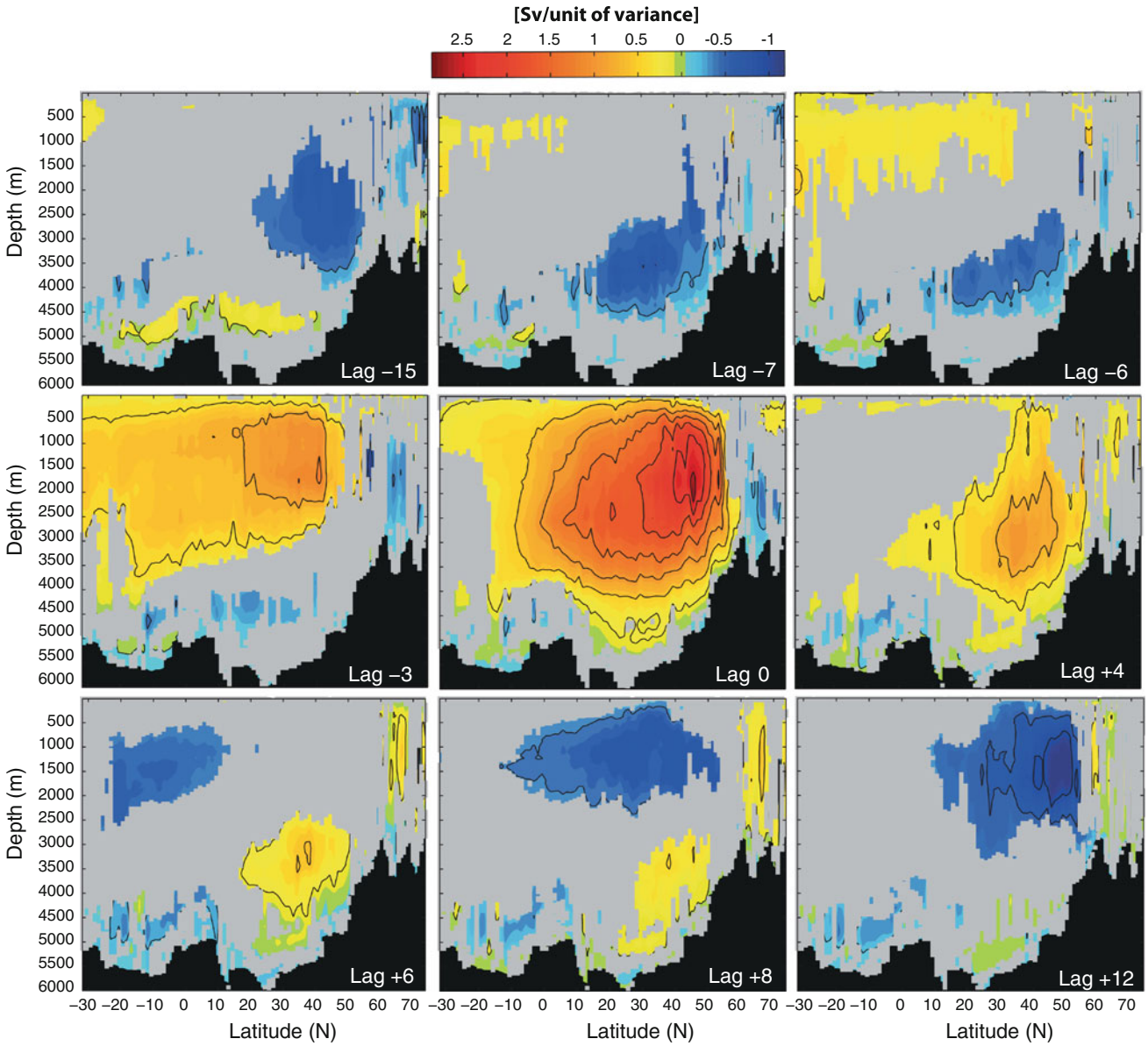

Fig. 6 Lead-Lag regression coefficient maps of the AMOC streamfunction (Fig. 3) at various lags to PC1 of the AMOC (Fig. 4b) [Sv unit of variance^{-1}]. The *grey shading* indicates 90 % confidence level for zero correlation

induced by AMOC fluctuations was obtained by averaging anomalies over years when the AMOC is strongest (i.e. when exceeding the AMOC standard deviation, Fig. 7). Significance of anomalies at each grid point was assessed by testing the null hypothesis that they were taken from a distribution that has the same mean as all the years (using a z test at the 90 % confidence level). When the AMOC is in its strong state, most of the upper ocean, from the subtropics to the mid-latitudes (mainly over the Gulf Stream path) and the Nordic Seas becomes warmer, whereas the northern tropics becomes significantly cooler. This cooling could be explained by the stronger heat transport associated with stronger AMOC conditions that takes away heat from the low latitudes towards the higher latitudes but also by associated changes in atmospheric forcing such as the NAO. The role of the atmosphere in this cooling is supported by the fact that the SST pattern has similarities with the structure of observed SST correlated with the NAO (e.g. Visbeck et al. 2001), and that at about 300–800 m depth this temperature pattern looks significantly different from the surface pattern (not shown). In CHIME, a northern tropical-subtropical SST dipole is identified, in contrast to HadCM3 where the SST dipole is cross-equatorial (Vellinga and Wu 2004). The difference in the dipoles probably results from differences in the SST patterns between the two models as identified by Megann

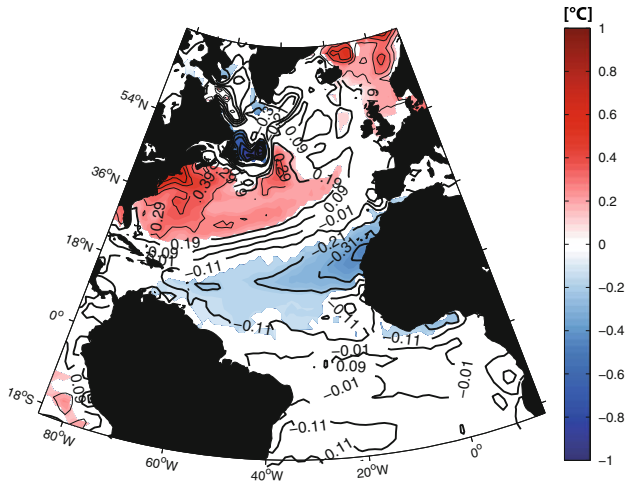

Fig. 7 Composite of winter anomaly patterns of SST induced by AMOC fluctuations, obtained by averaging anomalies over years when the AMOC (defined as the PC1 of the MOC) is strongest. *Colors* indicate where the null hypothesis of equal means is rejected at the 10 % level

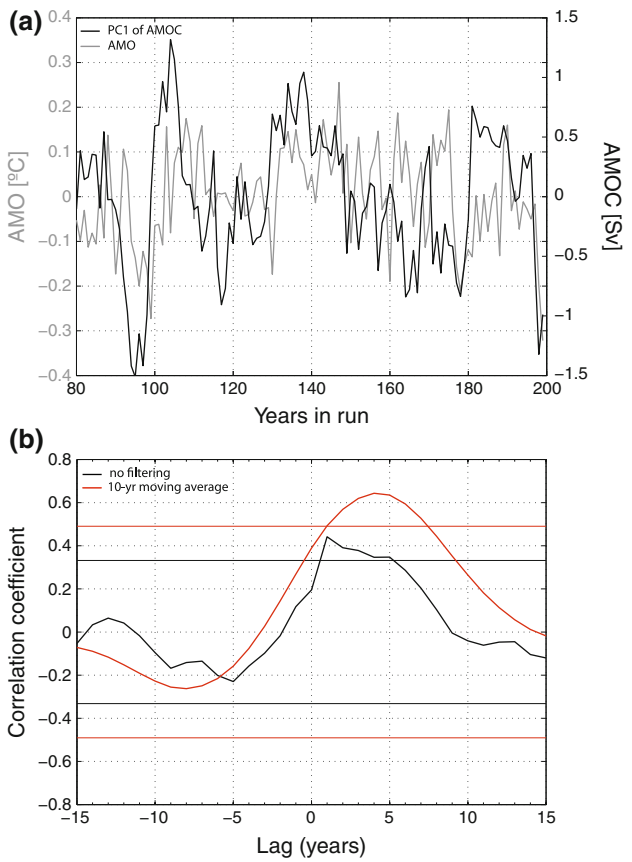

Fig. 8 Measures and relationships between AMO and AMOC indices: **a** time series of the area-averaged (90°W–30°E, 0°–70°N) annual SST anomaly after linear detrending (*grey line*), shown alongside the PC1 of AMOC (*black line*); **b** lagged cross-correlations plot between the two time series (*black line*) and their 10-year moving averaged time series (*red line*); *horizontal lines* correspond to their corresponding 95 % confidence limit for zero correlation. Positive lags are for PC1 leading the AMO

et al. (2010). A strong AMOC state in CHIME will therefore tend to warm the subtropics to the mid-latitudes and the Nordic Seas, and to cool the northern tropical SST, causing a northern tropical-subtropical SST gradient (a link strengthened by the strong and significant near-instantaneous correlation found between this gradient and the PC1 of AMOC, Table 1).

The leading mode of multi-decadal SST variability in the North Atlantic is known as the Atlantic Multi-decadal Oscillation (AMO, e.g. Kerr 2000), for which an index is traditionally defined as the basin-averaged (90°W–30°E, 0–70°N) SST anomaly (e.g. Knight et al. 2005), although the definition of AMO index might alternatively be defined in terms of the timescale of variability (Frankcombe et al. 2010). While the North Atlantic SST anomaly pattern in Fig. 7 is characterized as a sub-basin scale tropical-subtropical SST dipole, positive anomalies are predominant and the strongest in the Northern Hemisphere, suggesting an AMO-type response as seen in the observations (e.g. Sutton and Hodson 2005). This pattern is also somewhat reminiscent of SST anomaly patterns identified in previous studies as characteristic of multi-decadal variability on 20–30 year timescales (e.g. Figure 8 in Frankcombe et al. 2010). Figure 8a shows the AMO index (traditionally defined), after linear detrending (grey line), alongside our index for the leading (decadal) mode of AMOC variability (black line). On inspection, SST variability appears to lag AMOC variability. This is confirmed by lagged cross-correlations between the two time series, shown in Fig. 8b. The strongest and statistically most significant correlation is obtained when a 10-year moving average is applied to both time series; a maximum correlation of about 0.64 is for the PC1 of the AMOC leading the AMO by about 4 years (Fig. 8b, red line).

We further investigate the extent to which decadal variability in CHIME is associated with sub-surface thermal anomalies, as recently linked to observed multi-decadal variability (Frankcombe et al. 2008, 2010). Figure 9 shows sub-surface temperature anomalies (colour-shaded) as a function of longitude and time, averaged over CHIME layers 10–12 (spanning an approximate depth range 150–400 m in the subtropics) and the latitude range 10–30°N (best representative of westward propagation by layer anomalies). The time series at each longitude is de-trended and smoothed with a 5-year moving average. There is an overall impression of westward translation of sub-surface anomalies on a timescale of 7–10 years, similar in magnitude (±0.4 °C) to observations (Frankcombe et al. 2008).

In CHIME, layer temperature anomalies are accompanied by salinity anomalies (not shown) that have the

opposite effect on density, as layer densities below the mixed layer are prescribed. As a consequence, there is no associated density perturbation and these temperature and salinity anomalies are advected as passive tracers of water mass variability. A degree of westward propagation (in temperature and salinity) is associated with perturbations in layer thickness, although this is only clear over years 80–120. Anomalies in cumulative thickness of layers 10–12 (corresponding to the depth range of about 150–400 m), in the range ±10 m, are indicated in Fig. 9 by the over-plotted contours. These thickness anomalies are indicative of density anomalies, and are likely implicated in AMOC variability.

When and where layer interfaces are displaced anomalously upwards or downwards, the associated temperature and salinity anomalies may be substantial (reaching ±2.0 °C and ±0.5 psu), but inspecting animations of temperature and salinity anomalies at selected latitudes, these anomalies do not clearly propagate westwards for much of the period (consistent with the layer thickness anomalies in Fig. 9). In conclusion, the majority of sub-surface temperature variability seen to translate westwards does not cause AMOC variability but passively advects with the evolving velocity field. Averaged over the sub-tropics, temperature anomalies also spread downwards from a surface origin, on decadal timescales, accompanied by salinity anomalies that ensure constant layer density (not shown).

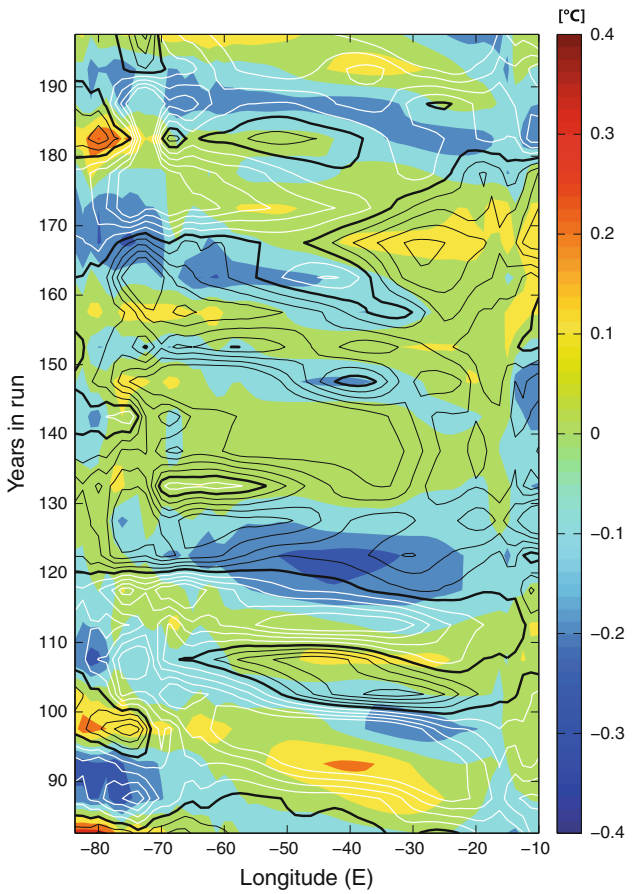

Fig. 9 Sub-surface anomalies as a function of longitude and time, averaged over CHIME layers 10–12 and the latitude range 10–30°N, detrended and smoothed with a 5-year moving average. Temperature anomalies are color-coded. Thickness anomalies are contoured, with a contour interval of 2.5 m (the zero *contour* is *bold*; positive anomalies are indicated by *thin black contours*; negative anomalies are indicated by *thin white contours*)

Previous studies have established that multi-decadal (20–30 year) variability may be understood as the thermal wind response to a surface thermal anomaly in the north-central part of the Atlantic basin, inducing westward Rossby wave propagation across the basin on near-decadal timescales (Colin de Verdière and Huck 1999), and subsequent adjustment of meridional temperature (hence density) gradients that lead to a dynamical response of the AMOC (te Raa and Dijkstra 2002). While westward translation of sub-surface temperature anomalies in the subtropics of CHIME appear on first inspection to be consistent with this mechanism, the accompanying salinity anomalies (in isopycnal layers) preclude any density perturbation. In contrast, thickness anomalies of ±10 m are a signature of interior density anomalies, but the associated temperature and salinity anomalies do not clearly propagate. We proceed in later sections to attribute the source of AMOC variability in CHIME to the advection of mixed layer salinity anomalies from low to sub-polar latitudes, while mixed layer temperature anomalies are strongly and quickly damped through surface heat fluxes. Regarding the latter process, there is however evidence for local correlation of anomalies in SST and surface heat flux associated with the NAO, as outlined in Sect. 5.3.2.

4.2 Atmosphere

Figure 10 shows composite atmospheric anomaly patterns when the AMOC is strongest, for winter anomalies of SAT, SLP, and September anomalies of net precipitation. Only significant values (at the 90 % level) are colored. When the AMOC is strongest, SAT along the western coast of North America (i.e. over the Gulf Stream path) and in the Nordic Seas becomes significantly warmer in contrast to both the northern tropics and the Labrador Sea areas where it becomes significantly cooler (Fig. 10a). This is consistent with the anti-phase relationship previously identified between the Labrador and GIN Seas (see Sect. 3.2). This SAT pattern somewhat resembles that of the SST in Fig. 7, and the anomalies vary from about 0.1 °C in the tropics and subtropics, to over 1 °C in the Nordic Seas. Over land, the strongest AMOC conditions are associated with a significant warming of northern Europe (in good agreement

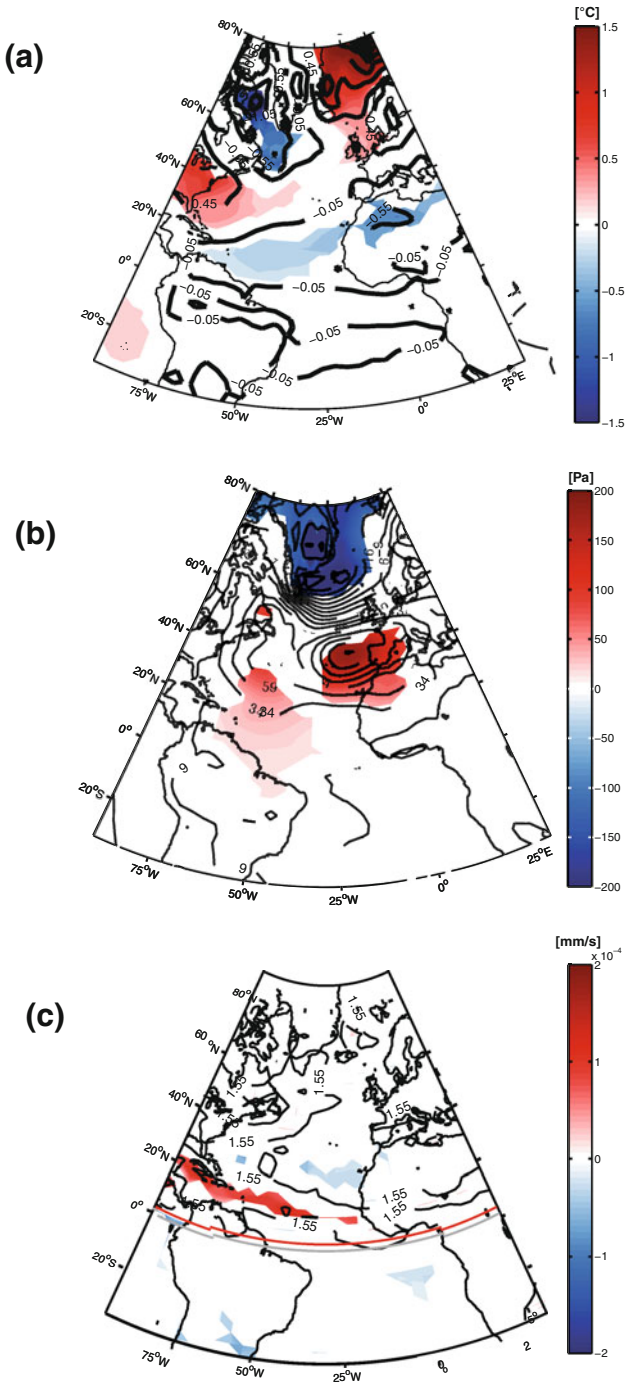

Fig. 10 Same as Fig. 7 but for **a** winter SAT [°C], **b** winter SLP [Pa] and **c** September net precipitation [mm s^{-1}] alongside with the averaged ITCZ position over both all the years (*grey line*) and years corresponding to strong AMOC conditions (*red line*). *Colors* indicate where the null hypothesis of equal means is rejected at the 10 % level

with e.g. Pohlmann et al. 2006) and the central eastern seaboard of North America.

Under the same strong AMOC conditions, lower SLP appears near the Icelandic Low, while higher SLP appears over the Azores (Fig. 10b). This pattern resembles the NAO, possibly reflecting some oceanic influence on this leading atmospheric mode. In CHIME, strong AMOC conditions therefore seem to be associated with a positive phase of the NAO. This NAO-like pattern is consistent with the NAO-like response to the AMOC intensification identified by Mignot and Frankignoul (2009) in the IPSL-CM4 model, although the sensitivity of SLP to changes in the AMOC in our model is about three times higher.

While few significant precipitation anomalies appear under strong AMOC conditions, some notable changes develop over the western tropics of the North Atlantic, with positive anomalies of up to 20 cm $year^{-1}$, suggesting a northward shift of the ITCZ (Fig. 10c), probably as a consequence of the tropical-subtropical SST gradient that accompanies strong AMOC conditions (Fig. 7). For a given year, the ITCZ position has been defined as the latitudinal position at which September precipitation reaches its maximum in the central Atlantic (i.e. at about 30°W, similar to Biasutti et al. 2006). We can see that the ITCZ position is indeed about 2.2° further north (red line) than the average position (grey line), which corresponds to a northward shift of about 230 km. With stronger precipitation expected north of the Equator, freshwater anomalies are expected to develop locally. A similar relationship between displacement of the ITCZ and lower frequency (centennial) variability of the AMOC has also been identified in HadCM3 by Vellinga and Wu (2004); however, in that study the northward shift of the ITCZ is caused by a cross-equatorial SST gradient, whereas in our case it seems to be associated with a northern tropical-subtropical SST gradient (see Fig. 7).

5 Physical mechanisms

5.1 Relation of AMOC to convective activity and density anomalies

If we examine how convective indices evolve over time in both the Labrador and GIN Seas (Fig. 4b, red and blue lines, respectively), an anti-phase relationship is clear, as already mentioned in Sect. 3.2. The maximum correlation coefficient of −0.7 is obtained for a slight lead, by 1 year, of convection in the Labrador Sea over that in the GIN Seas (Fig. 11). Correlation of these two convective indices with the PC1 of AMOC shows strong statistically significant relationships (Table 1); the Labrador (GIN) Sea(s) has a maximum (minimum) correlation coefficient of about 0.9 (−0.7) with the AMOC, when the latter lags by about 2 years (1 year). Note that the correlation is negative in the GIN Seas where it is positive in the Labrador Sea; an increase in MLD in the Labrador (GIN) Sea(s) is therefore associated with an increase (decrease) of the AMOC, 2 years (1 year) later.

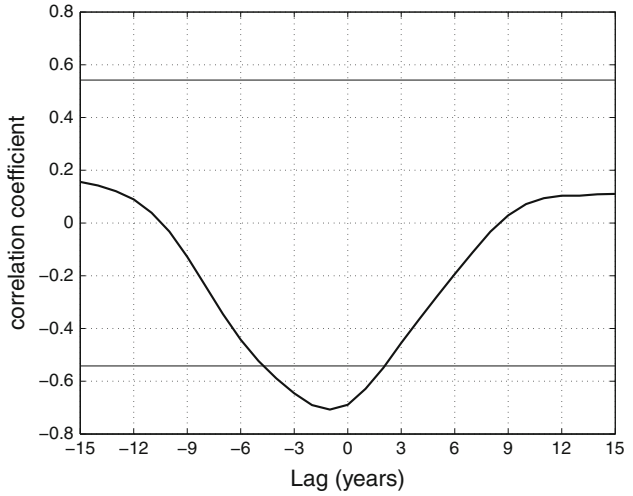

Fig. 11 Lagged cross-correlations plot between the 10-year moving average winter MLD in the Labrador and GIN Seas (positive lags for the GIN Seas leading the Labrador Sea); *horizontal black lines* correspond to the 95 % confidence limit for zero correlation

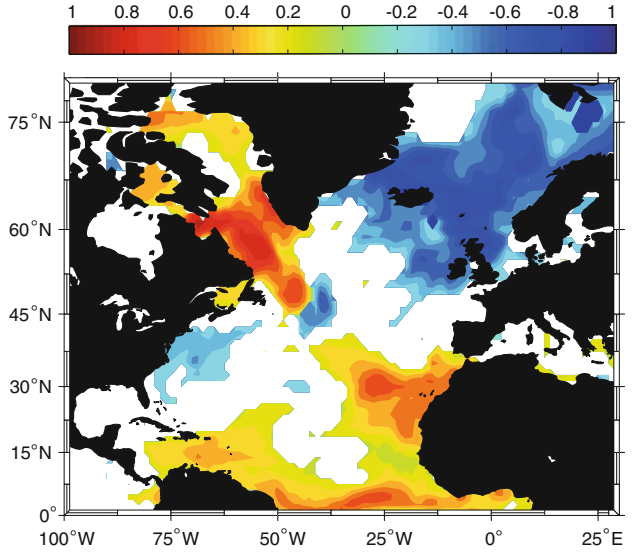

Fig. 12 Instantaneous correlation map of 10-year moving average of winter surface density and PC1 of AMOC. *Blank areas* are not statistically significant at the 95 % confidence level

In addition, if we examine how winter surface potential density (hence static stability) is spatially correlated (instantaneously) to AMOC fluctuations, the strongest correlations occur in both the Labrador and GIN Seas (Fig. 12). Correlations between winter surface density averaged over these two regions and AMOC fluctuations are very similar to those with the convective indices; surface density in the Labrador (GIN) Sea(s) is indeed strongly correlated (anti-correlated) with the AMOC intensity, with an average correlation coefficient of 0.86 (−0.83) (Table 1). There is therefore evidence that in CHIME, AMOC fluctuation is principally related to surface density in the Labrador Sea, reinforcing the suggestion that the first mode of AMOC variability (EOF1) is directly influenced by the convective activity in the Labrador Sea.

In summary, we have shown that surface density in the Labrador (GIN) Sea(s) is strongly correlated (anti-correlated) with AMOC fluctuations and explains about 64 % of the AMOC variance. Convective activity in the Labrador and GIN Seas in CHIME therefore varies in anti-phase; an increase in surface density in the Labrador (GIN) Sea(s) is associated with an increase (decrease) in the AMOC strength. This result is consistent with the opposite signs of EOF1 of the AMOC streamfunction, at the latitudes of Labrador and GIN Seas, seen in Fig. 4a. In the following section, we therefore investigate factors influencing surface density in the two convective regions.

5.2 Relative roles of temperature and salinity variability in driving density fluctuation

Figure 13 shows the influence of winter sea surface salinity (SSS) and SST on winter surface density fluctuations in both convective regions. In the GIN Seas, surface density is strongly anti-correlated with SST with a maximum instantaneous correlation of −0.93 (grey dashed line). A decrease in SST in the GIN Seas will therefore increase surface density in this region, while the role of SSS is negligible (grey solid line). In the Labrador Sea, by contrast, surface density is significantly correlated with SSS, with a maximum correlation of 0.8 when this latter leads by 3 years (black solid line). A decrease in SSS in the Labrador Sea will therefore most effectively decrease surface density in this region 3 years later, while in the meantime the role of SST is largely negligible (dashed black line).

Figure 14 shows the extent to which properties in these two convective regions are connected. Although both SST and SSS do not seem to be individually connected (see both dashed and solid grey lines), densities are significantly anti-correlated with a maximum coefficient of about −0.70 (black solid line) at no lag. This anti-correlation is again consistent with results from Sect. 5.1. This significant relationship between densities in these two convective regions exists despite the different mechanisms that seem to control them. Therefore we can expect that the process that controls the SSS in the Labrador Sea is anti-correlated to what causes changes in the SST in GIN Seas.

In summary, surface density changes in the Labrador Sea are salinity-dominated, while they are temperature-dominated in the GIN Seas. Different mechanisms are therefore likely to control surface density variability (with implications for the AMOC) in the two convective regions, although those mechanisms appear to be anti-correlated.

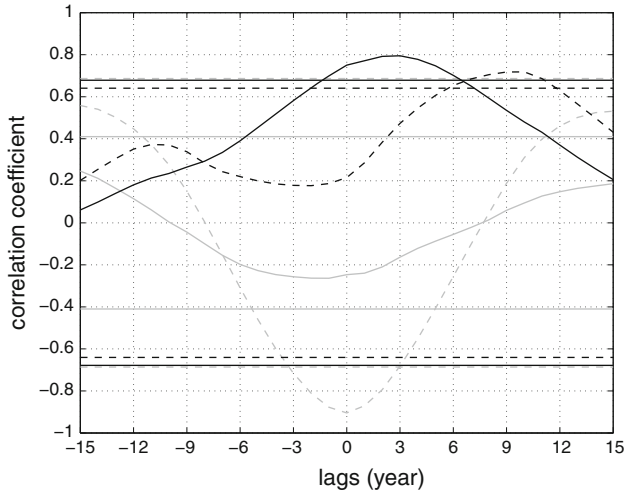

Fig. 13 Lagged cross-correlations plot of 10-year moving average between winter SSS (*solid lines*)/SST (*dashed lines*) and winter surface density in the Labrador Sea (*black lines*)/GIN Seas (*grey lines*). *Horizontal lines* correspond to their respective 95 % confidence limit for zero correlation

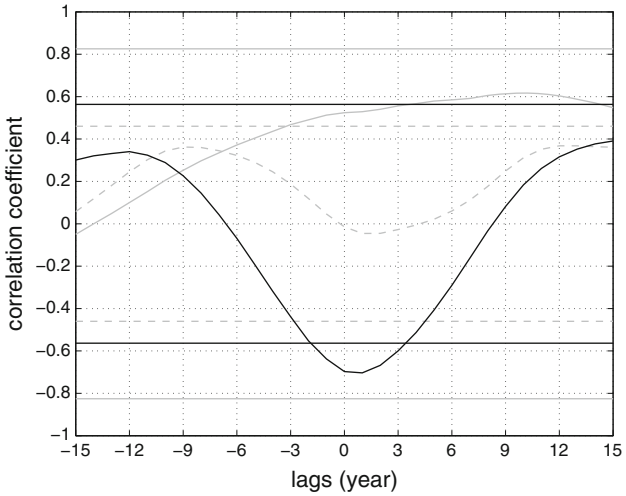

Fig. 14 Lagged cross-correlations plot of 10-year moving average between winter SSS (*grey solid line*), winter SST (*grey dashed line*), and winter surface density (*black solid line*) between the two convection regions (i.e. both the Labrador and GIN Seas). *Horizontal lines* correspond to their respective 95 % confidence limit for zero correlation

5.3 Origins of anomalies in convective regions

In this section, we investigate the origins of SST and SSS anomalies in both of the convective regions and the underlying oceanic and atmospheric processes.

5.3.1 Long-range preservation of salinity anomalies

Figure 15 shows maps of pentadal salinity anomalies from years 170 to 189 on three model layers in the upper branch of the AMOC, representative of the surface (Fig. 15a), and depth ranges around 90–150 m (Fig. 15b), and 200–650 m (Fig. 15c). These maps reveal how a positive salinity anomaly present in the tropics during the pentad 170–174 develops on a 15-year timescale. At the surface, the anomaly spreads northward along the Guyana Current and through the Caribbean, into the western subtropical gyre, and eventually into the interior of the subpolar gyre (Fig. 15a). This spreading is also evident at depth, where the anomaly reaches the deep convection regions after about 15 years (Fig. 15b,c). This is evidence for long-range preservation of salinity anomalies, en route from the tropics to the high latitudes, on a timescale of about 15 years.

The mechanism linking tropical and convective regions likely plays a role in the reversal phase of the AMOC oscillation. It is noteworthy that the AMOC appears to strengthen from low latitudes (see Fig. 6), suggesting an element of feedback as the salinity anomalies are also more rapidly advected northwards in the strengthening phase. As the AMOC dynamically evolves, transports start declining to the south, reducing the import of high salinity waters. Note that, this finding contrasts with several studies using the HadCM3 model where the reversal of the oscillation on multi-decadal timescales has been mainly attributed to anomalies originating from the high latitudes (e.g. Dong and Sutton 2005; Hawkins and Sutton 2007). Our finding is, however, consistent to some extent with Vellinga and Wu (2004), who showed that in HadCM3 the reversal oscillation is caused by anomalous advection of salinity anomalies from the tropics. But in their study, this happens on a centennial timescale rather than on a decadal timescale as identified in CHIME.

As previously shown in Sect. 5.2, salinity will predominantly affect surface density (with implications for the AMOC) in the Labrador Sea, while it does not directly affect density in the GIN Seas. Therefore, to obtain a better idea of how surface density in the Labrador Sea is correlated to salinity in the North Atlantic, linear lagged-correlation maps between salinity contributions to winter surface density in the Labrador Sea are analyzed (Fig. 16). The earliest correlations with SSS anomalies appear in the tropical West Atlantic (originating either from there or from the South Atlantic) about 15 years before a positive density anomaly in the Labrador Sea. With an AMOC cycle in the period range of 15–30 years (Sect. 3.1), this 15-year lead time corresponds to half of

Fig. 15 Pentadal anomalous salinity maps from year 170 to 189 on three model layers: **a** layer 1 (surface, constant-depth layer everywhere), **b** layer 9 ($\sigma_2 = 34.10$ kg m^{-3}, varying between about 90–150 m depth, non-isopycnic beyond 25°N), and **c** layer 14 ($\sigma_2 = 36.05$ kg m^{-3}, varying between about 200–650 m depth, non-isopycnic beyond 50°N) ▶

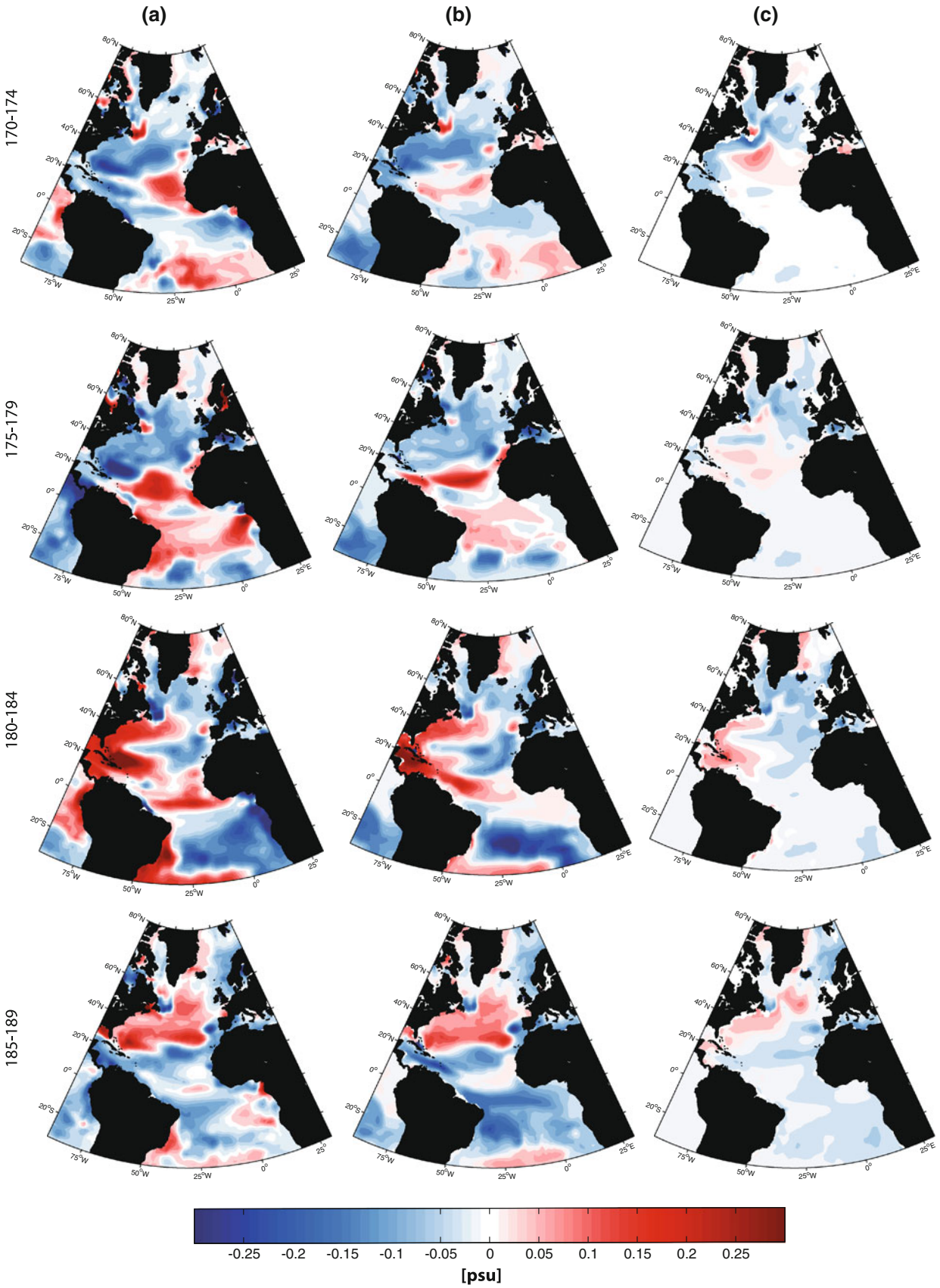
(a)
(b)
(c)
170-174
175-179
180-184
185-189
-0.25 -0.2 -0.15 -0.1 -0.05 0 0.05 0.1 0.15 0.2 0.25
[psu]

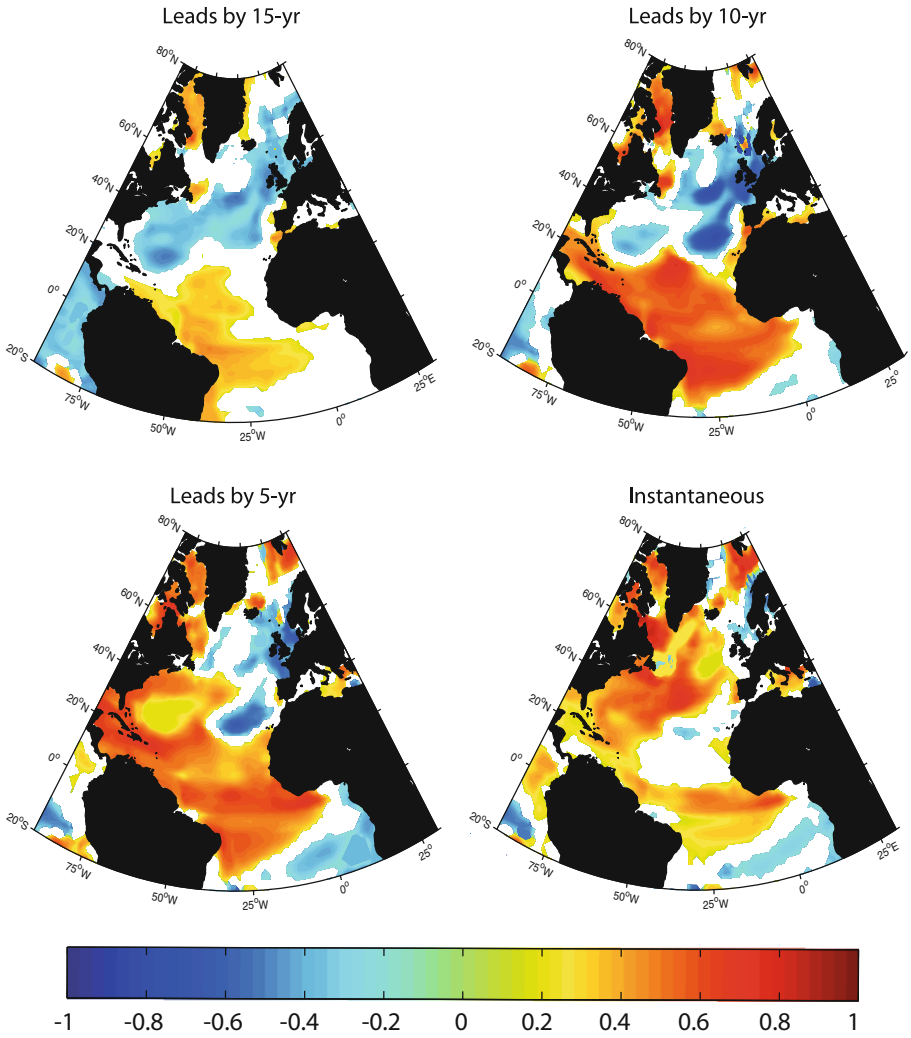

Fig. 16 Cross-correlations maps between annual SSS contributions and winter surface density in the Labrador Sea when SSS leads. *Blank areas* are not statistically significant at the 95 % confidence level

the maximum identified period of the longer decadal mode. At this stage, most of the northern North Atlantic is fresher than normal, consistent with the AMOC being in a weak phase. These fresh conditions gradually diminish and give way to more saline conditions over subsequent years, and the implication is that it takes about 15 years for the tropical positive anomalies to advect to the subpolar sinking region. These maps clearly reinforce the notion of northward transport of salinity anomalies, as previously shown.

In summary, SSS in the high-latitude regions seems to be strongly correlated to tropical SSS anomalies about 15 years earlier. These tropical anomalies will therefore also affect surface density in the Labrador Sea 15 years later while it will not be the case in the GIN Seas, where surface density is SST-dominated. There is therefore evidence for a 30-year cycle related to convective activity in the Labrador Sea in the primary mode of AMOC variability (EOF1) to be associated with the northward transport of northern tropical SSS anomalies.

5.3.2 Relative role of the NAO

As seen in Fig. 10b, strong AMOC conditions in CHIME are associated with a positive NAO-like pattern. In both the Labrador and GIN Seas, winter surface density has a statistically significant relationship with the NAO index (defined as the normalized pressure difference between Iceland and the Azores during the winter season), with a maximum positive correlation of 0.74 and negative correlation of −0.70, respectively, when the NAO leads by about 1–2 years (Table 2). The anti-phase behavior between the two convective regions in the model is once again underlined by these correlations of opposite sign. This result is consistent with observational studies, as convection in the Labrador Sea generally varies in phase with the NAO-index, while in the GIN Seas it varies out of phase (e.g. Hurrell and Dickson 2004). The above results therefore suggest that surface density in both the Labrador and GIN Seas is influenced by NAO fluctuations. This influence on AMOC variability has been extensively

Table 2 Maximum correlation coefficients between 10-year moving averages of the NAO index and several different variables

Variable	Max correlation coefficient	Lag (years)
Winter surface potential density (Labrador)	**0.74**	NAO leads by ~1–2
Winter surface potential density (GIN)	**−0.70**	NAO leads by ~1–2
Winter SST (GIN)	**0.70**	NAO leads by ~2
Winter SST (Labrador)	0.46	NAO lags by ~10
Winter SSS (Labrador)	0.46	NAO leads by ~4
Winter heat fluxes (GIN)	−0.15	NAO leads by ~5
Winter heat fluxes (Labrador)	**−0.60**	Instantaneous
Winter freshwater fluxes (GIN)	−0.45	NAO lags by ~7
Winter freshwater fluxes (Labrador)	**−0.65**	NAO leads by ~4–5
PC1 of AMOC	**0.82**	NAO leads by ~1
PC2 of AMOC	**−0.60**	Instantaneous
Tropical activity (TA)	**0.56**	NAO lags by ~8–9

Bold correlations are statistically significant at the 90 % confidence limits

investigated. The balance of evidence from previous modelling (e.g. Delworth and Greatbatch 2000; Eden and Willebrand 2001; Bentsen et al. 2004; Guemas and Salas-Mélia 2008) and observational studies (e.g. Dickson et al. 1996; Curry et al. 1998) suggests that both heat flux changes and wind-stress variations are important means by which the NAO influences the AMOC, across a wide range of frequencies.

In CHIME, the influence of the NAO on surface density in both convective regions seems to act through different processes. Indeed, although the NAO fluctuation explains about 50 % of SST variability in the GIN Seas ($r \sim 0.70$), no significant relationship with SST has been found in the Labrador Sea (Table 2). There is also no significant correlation between the NAO and SSS in the latter region, although SSS has been found to be the dominant factor influencing surface potential density there (see Sect. 5.2). Although we found evidence for the NAO to influence surface density through its impact on local SST in the GIN Seas, other processes seem to be involved in the Labrador Sea. Below, we consider regional NAO influences in more detail.

First let us consider the influence of the NAO on surface density in the Labrador Sea. We have shown the NAO to have statistically significant relationships with buoyancy fluxes in the Labrador Sea; an increase in the NAO index leads to a decrease in local surface heat fluxes (stronger ocean cooling) near-instantaneously ($r \sim -0.60$, Table 2) and to a decrease in freshwater fluxes (ocean freshwater loss) about 4–5 years later ($r \sim -0.65$, Table 2). Because the NAO affects surface density earlier (after ~1–2 years) than freshwater fluxes (after ~4–5 years), the NAO-induced freshwater flux anomalies cannot be regarded as directly influencing SSS (and therefore surface density) to an important extend in the Labrador Sea. However, with its near-instantaneous correlation with heat fluxes, the possibility of the NAO to influence local SSS through ocean mixing processes is not ruled out. In this scenario, the convective mixing associated with stronger surface heat loss will more extensively mix fresh surface waters with saline deep waters. In addition, the strong and significant anti-correlation found between SSS and heat fluxes in the Labrador Sea ($r \sim -0.72$ when heat fluxes lead by ~1 year, not shown) supports this mechanism.

In contrast to the case of the Labrador Sea, the NAO index does not correlate with surface heat and freshwater fluxes in the GIN Seas (Table 2). Therefore, the way by which the NAO affects local SST does not seem to be through its local impact on simultaneous heat fluxes. This can be further investigated by examining the covariance between anomalous SST and anomalous net surface heat flux ($\overline{T'Q'}$), noting that Q includes both radiative and turbulent heat fluxes, as shown in Fig. 17. If covariances are examined for the winter season of all years of the analysis period, significant values are observed in four main regions of the North Atlantic. Negative values occur over the Labrador Sea/western subpolar gyre and over the Greenland Sea, whilst positive values occur over the Florida Current/Gulf Stream region and over the upwelling region off West Africa. This implies that, over the oceanic deep convection regions, surface heat flux tends to damp SST variability (reducing temperature variance: in other words, positive SST anomalies result in increased oceanic heat loss). Further south, at the eastern and western boundaries of the subtropical gyre, the opposite is true and heat fluxes tend to amplify SST variability.

However, the simultaneous correlation contains contributions both from the atmospheric response to the SST (i.e. damping in this case) and also from the SST response to the atmosphere (Schneider and Fan 2007). We have calculated lag correlations between winter SST and heat flux during the previous summer (not shown). This does have positive

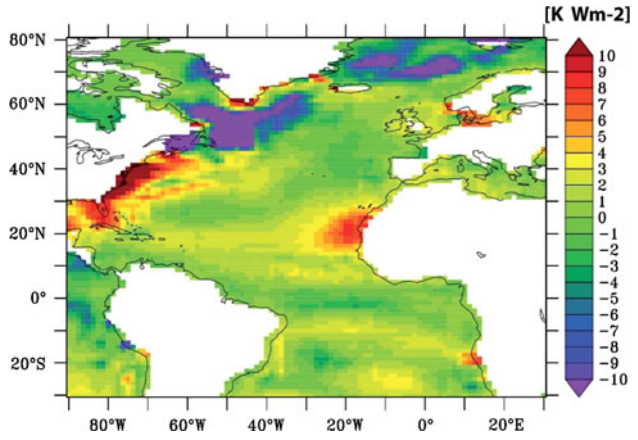

Fig. 17 SST-Heat Flux covariance ($\overline{T'Q'}$) in K Wm^{-2} calculated for winter mean anomalies over years 81–192 of the model experiment

values over the Greenland Sea, so we speculate that this may be a partial mechanism for the model correlation between the NAO and SST in the GIN Seas, although other processes such as advection and mixing may also be involved. Such a link between the NAO and SST may be more fully explored using a method such as the Interactive Ensemble Coupled GCM (Fan and Schneider 2012), but this lies beyond the scope of the present paper.

In CHIME, we therefore found evidence that the NAO strongly influences surface density in both the Labrador and GIN Seas (with implications for the AMOC) on interannual timescale but through different mechanisms. In summary, an increasing NAO index will lead to an increase in surface density in the Labrador Sea about 1–2 years later through a local (indirect) influence on SSS. By driving anomalous heat fluxes, the NAO forces variation of Labrador SSS through ocean mixing processes, and subsequently variations of the AMOC (as SSS is the dominant factor controlling surface density in this region). Meanwhile, an increasing NAO index will lead to a decrease in surface density in the GIN Seas about 1–2 years later through a local influence on SST. Processes other than the direct impact of the NAO on heat fluxes seem to control these local SST anomalies; the lagged response of surface heat fluxes (as discussed earlier) or the mechanical action of the NAO-induced wind (e.g. Pickart et al. 2003; Mignot and Frankignoul 2009) are regarded as plausible candidates. Note that a majority of previous studies (e.g. Curry et al. 1998; Delworth and Greatbatch 2000; Bentsen et al. 2004) showed that the link between the NAO and AMOC is via the restricted area of the Labrador Sea. This differs from our study, where a link between the atmosphere and the AMOC includes a statistically-significant relationship between the NAO index and surface density in the GIN Seas. This result however supports the finding of other studies, such as Dickson et al. (1996), Belkin et al. (1998), and Alekseev et al. (2001), that emphasize the importance of the GIN Seas in explaining the influence of the NAO on AMOC fluctuations.

The second mode of AMOC variability in CHIME, that we attributed to the interannual anti-phase variability related to convective activity in the Labrador Sea and the GIN Seas (see Sect. 3.2), thus seems to be associated with a local influence of the NAO on surface density in these two regions. The statistically significant correlation of −0.60 found between the NAO index and PC2 of the AMOC supports the above statement (Table 2). The implication is that a large part of the variability of the AMOC, being driven by the NAO, is a passive response to intrinsic internal atmospheric variability, rather than being part of a coupled ocean–atmosphere mode, and that this passive response to the atmosphere is associated mainly with the Labrador Sea. This is consistent with similarity of the AMOC PC1 power spectrum to that of red noise. However there is enhanced power in 15–30 year periods and we argue that this is due to advection of salinity anomalies from the tropics (Sect. 5.3.1 above) and links between the position of the ITCZ and the NAO (Sect. 5.3.3 below).

5.3.3 A link between tropical activity and NAO

In addition to the NAO-related mechanism affecting surface density in the GIN Seas, the close link between the convective activity in this latter region and the PC1 of the AMOC (see Sect. 3.2) also suggests the existence of a decadal-timescale mechanism affecting GSW variability. With evidence from previous studies that the North Atlantic climate variability is affected by tropical Atlantic ocean–atmosphere interaction (e.g. Rajagopalan et al. 1998; Okumura et al. 2001; Terray and Cassou 2002), we propose that the NAO and tropical activity are connected on a decadal timescale in our model.

We characterize the tropical activity (TA) in the Atlantic as the averaged September SSS over the northern tropical Atlantic (reflecting the northward shift of the ITCZ under strong AMOC conditions, leading to the development of freshwater anomalies in the northern tropics). In support of the above hypothesis (for an existing link between the tropics and the high latitudes in the model), TA is indeed statistically correlated with NAO variability with a maximum correlation coefficient of about 0.56 when TA leads by 8–9 years (Table 2). Although the mechanisms behind such a link still require clarification, this significant relationship suggests that the resultant upper-tropospheric divergence (caused by the anomalous shift of the ITCZ) affects the high latitude atmosphere (more specifically the NAO) about 8–9 years later, coincident with a decrease in surface density in the Labrador Sea and a decrease in SST (and hence increase in surface density) in the GIN Seas.

This connection between TA and NAO is consistent with previous studies (cited earlier).

In addition to the long-range preservation of SSS anomalies originating from the tropics and affecting LSW variability, the decadal cycle related to both LSW and GSW variability identified in the primary mode of AMOC variability (EOF1) therefore seems to be associated with mechanisms, still not clearly identified, that connect tropical activity to the NAO. The strong significant correlations found between the PC1 of the AMOC and both TA ($r = 0.75$, Table 1) and the NAO ($r = 0.82$, Table 2) confirm the above statement. With a lead-time of about 8–9 years, we note that this connection between the tropics and the high latitudes corresponds to just over half of the identified minimum period of the primary decadal mode of the AMOC (in the range 15–30 years).

6 Summary and discussion

We have analyzed the AMOC variability in a new coupled climate model, CHIME, using 121 years of model data after 80 years of spinup. CHIME features a hybrid-coordinate ocean component, but shares the same atmosphere and sea ice components as HadCM3, one of the most extensively used and studied climate models. This first study of natural variability in CHIME follows an initial study of the spinup and the equilibrium state in comparison with HadCM3 (Megann et al. 2010). The following summary and discussion covers three aspects of the study: (1) the characteristics of a strong AMOC state (prerequisite for understanding mechanisms behind decadal AMOC fluctuations); (2) the processes and lead/lag timescales implicated in the decadal variability of the AMOC; and (3) the specific differences between Atlantic decadal variability in CHIME and HadCM3 attributed to their different ocean components.

6.1 Fingerprints of a strong AMOC state

Strong AMOC conditions are associated with warmer SST over most of the North Atlantic from the subtropics to the high-latitudes, and cooler SST over the northern tropics. Despite being further north than other studies, this SST pattern (i.e. a northern tropical-subtropical gradient) reflects an AMO-type response in good agreement with previous studies (e.g. Sutton and Hodson 2005; Frankcombe et al. 2010). In sub-surface layers, temperature anomalies translate westwards and downwards in the subtropics, on decadal timescales. While this behaviour is also characteristic of the AMO (Frankcombe et al. 2008, 2010), we find that our index of mode-1 AMOC variability leads the AMO index by 2–3 years, suggesting that, in CHIME at least, sub-surface temperature variability is a response to AMOC variability rather than a cause. Accompanying sub-surface salinity anomalies exactly compensate for the temperature anomalies in isopycnic layers, and the small perturbations in horizontal density gradients (in the subtropics) that are associated with layer thickness anomalies do not appear to lead AMOC anomalies.

Strong AMOC conditions tend to coincide with warm SAT from the subtropics to the high latitudes, except in the Labrador Sea where it becomes cooler. Over land, parts of northern Europe and central North America also become warmer. Coincident with the strong AMOC are also a positive-state NAO and maximum northward shift of the ITCZ. Associated with the positive NAO are positive surface heat flux anomalies (reduced ocean heat loss) which reinforce higher SST in the GIN Seas, helping to suppress convection (see Sect. 6.2). With northward displacement of the ITCZ and associated net surface freshwater influx ($P-E > 0$), a negative anomaly develops in surface salinity across the tropics.

6.2 Key processes implicated in decadal AMOC fluctuations

Power spectral analysis reveals an enhanced power at a decadal timescale in CHIME, for periods in the range 15–30 years. Overall, the main modes of variability are described by changes associated with primarily a decadal cycle and secondarily an interannual cycle related to convective activity in the Labrador and (inversely) the GIN Seas. Accompanying decadal AMOC variability are anomalies in basin-scale hydrography and air-sea heat fluxes at key locations. Associated variability in the atmosphere includes the NAO (varying in phase with the AMOC) and the ITCZ (migrating north/south with a strengthening/weakening AMOC).

An out-of-phase relationship in MLD between sinking regions indicates that strong sinking in the Labrador Sea is coincident with weak sinking in the GIN Seas, associated with positive and negative surface density anomalies respectively. Positive density anomalies in the Labrador Sea are associated with anomalously high surface salinity, while negative density anomalies in the GIN Seas are associated with anomalous surface warmth. Therefore, SSS (SST) anomalies in the GIN (Labrador) Seas are negligible compared to SST (SSS) in affecting surface density, and hence AMOC fluctuations.

Surface salinity in the Labrador Sea (and hence surface density) appears to be associated with the northward spreading of anomalies originating from the tropical Atlantic around 15 years earlier. Tropical SSS anomalies may have formed locally through air-sea interaction as a consequence of the ITCZ shift, leading to anomalous

surface freshwater gain in the northern tropical Atlantic under strong AMOC conditions. Although a significant shift of the ITCZ has been identified in the model, other processes responsible for the development of SSS anomalies are not to be excluded such as changes in the Amazon River outflow, or inter-basin exchange (Biastoch et al. 2008, 2009). In addition, there is evidence for the anomalous shift of the ITCZ (and its resultant upper-tropospheric divergence) affecting the high-latitude atmosphere, more specifically the NAO about 8–9 years later. Although mechanisms behind such a link remain unclear, previous studies emphasize a teleconnection excited by anomalous shifts in the Atlantic ITCZ, forcing a barotropic response that modulates the strength of the North Atlantic subtropical high and the northeast trades (Okumura et al. 2001; Sutton et al. 2001; Terray and Cassou 2002). This change in NAO forcing will first near-instantaneously affect heat fluxes in the Labrador Sea, which in turn will affect (increase) local SSS (and hence surface density) through ocean mixing processes. In the meantime, NAO will near-instantaneously impact SST in the GIN Seas, although the precise mechanism for this is still unclear. To summarise, in a positive (negative) NAO state, coincident with strong (weak) AMOC conditions, orientation of the Atlantic storm track will favour warmer (colder) conditions in the GIN Sea and saltier (fresher) conditions in the Labrador Sea.

In CHIME, we therefore found evidence for surface density in both the Labrador Sea and the GIN Seas to be influenced by the tropical activity about a decade earlier but through different mechanisms. The fact that one unit change of surface density in the GIN Seas has stronger impact on AMOC fluctuations than one unit change in the Labrador Sea (about 14 and 7 Sv kg^{-1} m^3, respectively) and that the Labrador Sea has in contrast a dominant influence on AMOC strength (as shown by their positive correlations) suggests that variability in the latter region is higher than in the GIN Seas. To summarize, a relatively fast atmospheric teleconnection may link ITCZ changes to the NAO, affecting the surface density in the GIN Seas, while both atmospheric teleconnection (hence the NAO) and slower ocean advection (of tropical SSS anomalies) affect surface density in the Labrador Sea. Which of these processes is more important in controlling decadal AMOC variability? Our results show that the first principal component of the AMOC has a slightly stronger correlation with the NAO index ($r = 0.82$, Table 2) than the northern tropical-subtropical SST gradient (resulting in a shift of the ITCZ) ($r = 0.79$, Table 1), suggesting that the NAO-related mechanism is slightly dominant. We also emphasize that, although the processes described above contribute to AMOC variability on decadal timescales, a large part of the variability of the AMOC is likely to be a passive response to intrinsic internal atmospheric variability (in common with most climate models, e.g. Delworth et al. 1993; Dong and Sutton 2005), rather than being part of a coupled ocean–atmosphere mode (e.g. Timmerman et al. 1998).

6.3 Comparing decadal variability in CHIME and HadCM3

As CHIME shares identical atmosphere and sea ice components with HadCM3, we can assess the extent to which the choice of vertical representation of the ocean affects decadal AMOC variability in the two models. Here, we summarize the main differences between the two models based on the present study and previous similar studies using HadCM3.

It has been shown that AMOC oscillations are mostly irregular and their periods change considerably among models; while ECHAM5/Max Planck Institude Ocean Model (MPI-ON; Jungclaus et al. 2005) has one of the longest periods with 70–80 years, HadCM3 (Dong and Sutton 2005) and Parallel Climate Model (PCM; Dai et al. 2005) show the shortest periods with about 25 years. While it has been difficult to estimate the period of AMOC variability in CHIME due to limited integration length, its power spectra nevertheless revealed an enhanced power for periods in the range 15–30 years. CHIME therefore shows a low-range period of AMOC variability that includes the 25-year period found in HadCM3. Although longer CHIME integrations are needed to better establish this range of periodicity, our evidence suggests that CHIME and HadCM3 share similar-period AMOC oscillations. In both CHIME and HadCM3, the circulation associated with the NADW has a maximum transport of about 18 Sv, well within the CMIP3 range (10–30 Sv, Gregory et al. 2005). There are, however, some structural differences in the respective meridional overturning streamfunctions. In CHIME, for example, the strongest sinking occurs in a broader region (between about 55°N and 65°N) than in HadCM3 (primarily occurring at 65°N, Dong and Sutton 2005). Megann et al. (2010) explained that this difference could be partly due to the deeper mixing in the subpolar gyre in CHIME and to the reduced mixing in the Labrador Sea in HadCM3. Note, however, that compared to observations, CHIME overestimates winter mixed layer depth in the Labrador Sea while HadCM3 underestimates it. The AMOC also comprises NADW outflow of about 16 Sv at the Equator in CHIME against 14 Sv in HadCM3 (Dong and Sutton 2005), and the outflow extends deeper in CHIME (to about 4,000 m, against 3,600 m in HadCM3, Megann et al. 2010).

In addition, the dominant mode of AMOC variability in CHIME has a spatial structure very similar to that in HadCM3, and the amount of total variance explained is similar in both models (about 34 %, Dong and Sutton

2005; Bingham et al. 2007). There are nevertheless significant differences; for example, the maximum value for a fluctuation of one standard deviation of PC1 is more than double in CHIME (about 1.6 Sv) compared to HadCM3 (about 0.7 Sv). Another significant difference is that the phases of EOF1 in the Labrador Sea and Nordic Seas are of opposite sign in CHIME while they remain similar in HadCM3 (Dong and Sutton 2005; Bingham et al. 2007), with the caveat that Labrador Sea convection is much weaker in HadCM3 than in CHIME. In that sense, CHIME seems more realistic; in observational studies, it has been established that convection in the Labrador Sea is generally out of phase with convection in the Greenland Sea (e.g. Hurrell and Dickson 2004). Therefore, different mechanisms appear to control AMOC variability on decadal timescales in CHIME and HadCM3.

On a decadal timescale, phase reversal of the AMOC oscillation in CHIME seems linked to salinity anomalies in the tropics. As already mentioned in Sect. 5.3.1, this finding contrasts with several studies using HadCM3 where the reversal oscillation has been mainly attributed to anomalies originating from high latitudes (Hawkins and Sutton 2007; Dong and Sutton 2005) but is to some extent in good agreement with Vellinga and Wu (2004) who attributed this reversal oscillation to advection of salinity anomalies from the tropics. However, this advection happens on a centennial timescale rather than on the decadal timescale identified in CHIME. A plausible explanation of the faster advection of anomalies in CHIME could come from the better preservation of water masses, compared to HadCM3 (as discussed by Megann et al. 2012); so an anomalous water mass maintains its structure better in CHIME, and can be more effectively advected "intact" to the high latitudes. Note, however, that centennial mechanisms (as identified by Vellinga and Wu 2004) may also be active in CHIME but these cannot be investigated with the short integration available to us. Tropical salinity anomalies in CHIME may be a consequence of a northward shift of the ITCZ associated with strong AMOC conditions, as also identified in HadCM3, although the cause of this shift is due to a northern tropical-subtropical SST gradient and not to a cross-equatorial SST gradient as identified in HadCM3 (Vellinga and Wu 2004) and observations (e.g. Chiang et al. 2002). This more northward SST gradient in CHIME may be a consequence of the strong warm surface bias in the North Atlantic (Megann et al. 2010). Despite these differences, CHIME is similar to HadCM3 (Dong and Sutton 2005) in that a significant part of the AMOC variability is likely to be a passive response to the internally generated atmospheric variability.

In CHIME, we have therefore identified the apparent long-range preservation of salinity anomalies originating from the tropics and advecting towards the high latitudes on a timescale shorter than in HadCM3. However, to substantiate the realism of salinity preservation and the speed of the northward advection of anomalies in CHIME, it would be necessary to undertake comparisons with multi-decadal observations. Such observations are at present inadequate for this purpose, due to under-sampling of much of the Atlantic sector prior to the Argo era. To further establish the extent to which these features (i.e. salinity preservation and speed of northward advection) are particular to CHIME, it would be necessary to undertake a more in-depth intercomparison with a climate model typical of the majority that feature a more orthodox z-coordinate ocean component. In comparison with HadCM3, the early evidence is that CHIME does indeed better preserve the properties of intermediate waters such as Antarctic Intermediate Water, over long distances (Megann et al. 2010). However, HadCM3 may not be the most appropriate model for such comparison, due to the limited role that Labrador Sea convection plays in driving AMOC variability in this model.

7 Conclusions

The sequence of events based on the range of statistical evidence presented in previous sections allows us to schematically summarize the main processes implied in about one half of a decadal-timescale AMOC cycle primarily driven by the Labrador Sea in CHIME, as shown in Fig. 18. Strong AMOC conditions are accompanied by the development of freshwater anomalies in the northern tropics (as a consequence of the northward shift of the ITCZ). Accompanying this variation of tropical SSS, concurrent changes in the tropical atmosphere lead to a decrease in the NAO about 8–9 years later, via a rapid atmospheric teleconnection. This weaker NAO decreases surface density (and hence SSS) in the Labrador Sea, through reduction in surface heat loss and the convective mixing of fresh surface and saline deep waters. Simultaneously, surface density will increase in the GIN Seas, due to decreased SST, possibly through the mechanical action of the NAO-induced wind (Pickart et al. 2003; Mignot and Frankignoul 2009) or a lagged response to increases in surface heat loss. Meanwhile, northward transport of freshwater anomalies from the tropics to the high-latitudes, via the Gulf Stream, further decreases SSS in the Labrador Sea and hence surface density in this region. Associated with increased (decreased) surface density in the GIN (Labrador) Seas, the AMOC is now in a weak state.

In conclusion, variability in the Atlantic sector of CHIME can be summarized in the following key points:

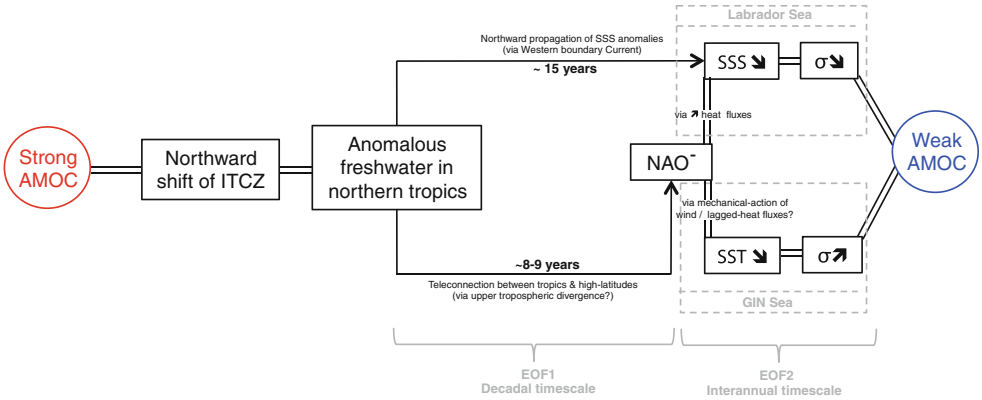

Fig. 18 Simplified schematic of mechanism responsible for one half of the decadal AMOC cycle primarily driven by the Labrador Sea variability in CHIME. *Double lines* are used when the timescale of the interaction is near-instantaneous (<3-years)

- The primary mode of AMOC variability is associated with decadal LSW and GSW variability, both linked to changes in tropical activity about a decade earlier, but through different mechanisms: (1) Decadal GSW variability is controlled by the low-frequency NAO variability that may result from a rapid atmospheric teleconnection, from tropics to the extratropics, of changes on a 10-year timescale (associated with anomalous shifts of the ITCZ and the accompanying upper-tropospheric divergence); (2) In addition to the NAO-related mechanism, decadal LSW variation is also influenced by the northward advection of tropical SSS anomalies on a 15-year timescale (associated with changes in ITCZ position).
- The secondary mode of AMOC variability is associated with interannual LSW and GSW variability through the influence of higher-frequency NAO variability on surface density in both the Labrador and GIN Seas, but involving different mechanisms.

The long-range links between the tropical Atlantic activity and subsequent convective activity in both the Labrador and GIN Seas regions in CHIME suggest that European climate is potentially predictable on substantially longer timescales than the 5–10 years typically asserted from experiments with climate models that feature an orthodox z-level coordinate ocean component (e.g. Latif et al. 2006). Potential predictability studies with this hybrid-coordinate ocean component model are therefore the subject of ongoing work.

Acknowledgments This work is funded under the "Strategic Ocean Funding Initiative" (SOFI) of the NERC Oceans 2025 research programme (Grant # NE/F012241/1). We also acknowledge the RAPID-THCMIP project. The authors are grateful to Juliette Mignot, Eric Guilyardi and Claude Frankignoul at LOCEAN (Institut Pierre-Simon Laplace, Jussieu, Paris) for their useful comments. We finally thank the editor and two anonymous reviewers for insightful remarks and constructive suggestions that led to substantial improvement of the manuscript.

References

Alekseev GV, Johannessen OM, Korablev AA, Ivanov VV, Kovalesky DV (2001) Interannual variability of water mass in the Greenland Sea and the adjacent areas. Polar Res 20:207–210

Belkin IM, Levitus S, Antonov JI, Malmberg SA (1998) "Great Salinity Anomalies" in the North Atlantic. Prog Oceanogr 41:1–68

Bentsen M, Drange H, Furevik T, Zhou T (2004) Simulated variability of the Atlantic meridional overturning circulation. Clim Dyn 22. doi:10.1007/s00382-004-0397-x

Biastoch A, Böning CW, Lutjeharms JRE (2008) Agulhas leakage dynamics affects decadal variability in Atlantic overturning circulation. Nature 456:489–492. doi:10.1038/nature07426

Biastoch A, Böning CW, Schwarzkopf FU, Lutjeharms JRE (2009) Increase in Agulhas leakage due to poleward shift in the southern hemisphere westerlies. Nature 462:495–498. doi:10.1038/nature08519

Biasutti M, Sobel AH, Kushnir Y (2006) GCM precipitation biases in the tropical Atlantic. J Clim 19:935–958

Bingham RJ, Hughes CW, Roussenov V, Williams RG (2007) Meridional coherence of the North Atlantic meridional overturning circulation. Geophys Res Lett 34:L23606. doi:10.1029/2007GL031731

Bleck R (2002) An oceanic general circulation model framed in hybrid isopycnic-Cartesian coordinates. Ocean Mod 4:55–88

Chatfield C (1975) The analysis of timeseries: theory and practice. Chapman and Hall, London

Chiang JC, Kushnir Y, Giannini A (2002) Deconstructing Atlantic intertropical convergence zone variability: influence of the local cross-equatorial sea surface temperature gradient and remote forcing from the eastern equatorial Pacific. Geophys Res Lett 107:4004. doi:10.1029/2000JD000307

Colin de Verdière A, Huck T (1999) Baroclinic instability: an oceanic wavemaker for interdecadal variability. J Phys Oceanogr 29:893–910

Curry RG, McCartney MS, Joyce TM (1998) Oceanic transport of subpolar climate signals to mid-depth subtropical waters. Nature 391:575–577

Dai A, Hu A, Meehl GA, Washington WM, Strand WG (2005) Atlantic thermohaline circulation in a coupled general circulation model: unforced variations versus forced changes. J Clim 18:3270–3293

Danabasoglu G (2008) On multi-decadal variability of the Atlantic meridional overturning circulation in the Community Climate System Model Version 3 (CCSM3). J Clim 24:5524–5544

Delworth TL, Greatbatch RJ (2000) Multidecadal thermohaline circulation variability driven by atmospheric surface flux forcing. J Clim 13:1481–1495

Delworth TL, Mann ME (2000) Observed and simulated multidecadal variability in the Northern Hemisphere. Clim Dyn 16:661–676

Delworth TL, Manabe S, Stouffer RJ (1993) Interdecadal variations of the thermohaline circulation in a coupled ocean-atmosphere model. J Clim 6:1993–2011

Dickson RR, Lazier J, Meincke J, Rhines P, Swift J (1996) Long-term coordinated changes in the convective activity of the North Atlantic. Prog Oceanogr 38:241–295

Dong B, Sutton RT (2005) Mechanism of interdecadal thermohaline circulation variability in a coupled ocean- atmosphere GCM. J Climate 18:1117–1135

Eden C, Willebrand J (2001) Mechanism of interannual to decadal variability of the North Atlantic Circulation. J Clim 14:2266–2280

Fan M, Schneider EK (2012) Observed decadal North Atlantic tripole SST variability. Part I: weather noise forcing and coupled response. J Atmos Sci 69:35–50

Frankcombe LH, Dijkstra HA, von der Heydt A (2008) Sub-surface signatures of the Atlantic multidecadal oscillation. Geophys Res Lett 35:L19602. doi:10.1029/2008GL034989

Frankcombe LH, von der Heydt A, Dijkstra HA (2010) North Atlantic multidecadal climate variability: an investigation of dominant time scales and processes. J Clim 23:3626–3638

Ganachaud A, Wunsch C (2000) Improved estimates of global ocean circulation, heat transport and mixing from hydrographic data. Nature 408:453–457

Gordon AL, Zebiak SE, Bryan K (1992) Climate variability and the Atlantic Ocean. Eos Trans AGU 73:161–165

Gordon C, Cooper C, Senior CA, Banks H, Gregory JM, Johns TC, Mitchell JFB, Wood RA (2000) The simulation of SST, sea ice extents and ocean heat transports in a version of the Hadley Centre coupled model without flux adjustments. Clim Dyn 16:147–168

Gregory JM et al (2005) A model intercomparison of changes in the Atlantic thermohaline circulation in response to increasing atmospheric CO2 concentration. Geophys Res Lett 32:L12703. doi:10.1029/2005GL023209

Guemas V, Salas-Mélia D (2008) Simulation of the Atlantic meridional overturning circulation in an atmosphere–ocean global coupled model. Part I: a mechanism governing the variability of ocean convection in a preindustrial experiment. Clim Dyn 31:29–48

Hawkins E, Sutton R (2007) Variability of the Atlantic thermohaline circulation described by three-dimensional empirical orthogonal functions. Clim Dyn 29:745–762

Herweijer C, Seager R, Winton M, Clement A (2005) Why the ocean heat tranport warms the global mean climate. Tellus 57A:662–675

Hurrell JW, Dickson RR (2004) Climate variability over the North Atlantic. In: Stenseth NC et al (eds) Marine ecosystems and climate variation. Oxford University Press, Oxford, pp 15–31

Jungclaus J, Haak H, Latif M, Mikolajewicz U (2005) Arctic-North Atlantic interactions and multidecadal variability of the meridional overturning circulation. J Clim 18:4013–4031

Kerr RA (2000) A North Atlantic climate pacemaker for the centuries. Science 288:1984–1985

Knight JR, Allan RJ, Folland CK, Vellinga M, Mann ME (2005) A signature of persistent natural thermohaline circulation cycles in observed climate. Geophys Res Lett 32:L20708. doi:10.1029/2005GL024233

Latif M, Roeckner E, Botzet M, Esch M, Haak H, Hagemann S, Jungclaus J, Legutke S, Marsland S (2004) Reconstructing, monitoring, and predicting multidecadal-scale changes in the North Atlantic thermohaline circulation with sea surface temperature. J Clim 17:1605–1614

Latif M, Collins M, Pohlmann H, Keenlyside N (2006) A review of predictability studies of Atlantic sector climate on decadal time scales. J Clim 19:5971–5986

Levitus S (1998) World Ocean Atlas, US Department of Commerce

Megann AP, New AL, Blaker AT, Sinha B (2010) The sensitivity of a coupled climate model to its ocean component. J Climate 23:5126–5150

Megann AP, New AL, Blaker AT (2012) The effect of interannual-timescale salinity anomalies on the stability of the Atlantic meridional overturning circulation. Clim Dyn (under review)

Mignot J, Frankignoul C (2005) The variability of the Atlantic meridional overturning circulation, the north atlantic oscillation, and the el nino southern oscillation in the Bergen climate model. J Clim 18(13):2361–2375

Mignot J, Frankignoul C (2009) Local and remote impacts of a tropical Atlantic salinity anomaly. Clim Dyn. doi: 10.1007/s00382-009-0621-9

Okumura Y, Xie SP, Numaguti A, Tanimoto Y (2001) Tropical Atlantic air–sea interaction and its influence on the NAO. Geophys Res Lett 28:1507–1510

Pickart RS, Spall MA, Ribergaard MH, Moore GWK, Milliff RF (2003) Deep convection in the Irminger Sea forced by the Greenland tip jet. Nature 424:152–156

Pohlmann H, Sienz F, Latif M (2006) Influence of the multidecadal Atlantic meridional overturning circulation variability on European climate. J Clim 19:6062–6067

Rajagopalan B, Kushnir Y, Tourre YM (1998) Observed mid-latitude and tropical Atlantic climate variability. Geophys Res Lett 25:3967–3970

Reid JL (1989) On the total geostrophic circulation of the South Atlantic Ocean: flow patterns, tracers, and transports. Prog Oceanogr 23:149–244

Roberts MJ, Marsh R, New AL, Wood RA (1996) An intercomparison of a Bryan-Cox type ocean model and an isopycnic ocean model. Part I: the subpolar gyre and high latitude processes. J Phys Oceanogr 26:1495–1527

Santer BD, Wigley TML, Barnett TP, Anyamba E (1996) Detection of climate change and attribution of causes. In: Callander BA, Harris N, Kattenberg A, Houghton JT, Meira Filho LG (eds) Climate change 1995. The IPCC second scientific assessment. Cambridge University Press, Cambridge, pp 407–444

Schmitz WJ Jr, Richardson PL (1991) On the sources of the Florida current. Deep-Sea Res 38(Suppl 1):S389–S409

Schneider EK, Fan M (2007) Weather noise forcing of surface climate variability. J Atmos Sci 64:3265–3280

Sun S, Bleck R (2001) Thermohaline circulation studies with an isopycnic coordinate ocean model. J Phys Oceanogr 31:2761–2782

Sutton RT, Hodson DLR (2005) Atlantic Ocean forcing of North American and European summer climate. Science 309:115–118

Sutton RT, Norton WA, Jewson SP (2001) The North Atlantic Oscillation—what role for the ocean? Atmos Sci Lett 1(2). doi: 10.1006/asle.2000.0018

Talley LD (2003) Shallow, intermediate, and deep overturning components of the global heat budget. J Phys Oceanogr 6333:530–560

te Raa LA, Dijkstra HA (2002) Instability of the thermohaline circulation on interdecadal timescales. J Phys Oceanogr 32:138–160

Terray L, Cassou C (2002) Tropical atlantic sea surface temperature forcing of the quasi-decadal climate variability over the north Atlantic-Europe region. J Clim 15:3170–3187

Timmerman A, Latif M, Voss R, Grötzner A (1998) Northern Hemisphere interdecadal variability. J Clim 11:1906–1931

Vellinga M, Wu P (2004) Low-latitude freshwater influence on centennial variability of the Atlantic thermohaline circulation. J Clim 17:4498–4511

Visbeck MH, Hurrell JW, Polvani L, Cullen HM (2001) The North Atlantic oscillation: past, present, and future. Proc Natl Acad Sci USA 98:12876–12877

Von Storch H, Zwiers FW (1999) Statistical analysis in climate research. Cambridge University Press, Cambridge, p 494

Winton M (2003) On the climatic impact of ocean circulation. J Clim 16:2875–2889